Received: 25 August 2021 | Revised: 10 September 2021 | Accepted: 10 September 2021

DOI: 10.1111/jace.18125

Journal of the American Ceramic Society

RESEARCH ARTICLE

Lead silicate glass structure: New insights from diffraction and modeling of probable lone pair locations

Oliver L. G. Alderman[1,#] | **Alex C. Hannon**[1] | **Diane Holland**[2] | **Ray Dupree**[2] | **Gloria Lehr**[3] | **Adam Vitale**[3] | **Steve Feller**[3]

[1] ISIS Neutron and Muon Source, Rutherford Appleton Laboratory, Oxon, UK

[2] Department of Physics, University of Warwick, Coventry, UK

[3] Physics Department, Coe College, Cedar Rapids, USA

Correspondence
Oliver L. G. Alderman and Alex C. Hannon, ISIS Neutron and Muon Source, Rutherford Appleton Laboratory, Chilton, Didcot, Oxon OX11 0QX, UK.
Email: oliver.alderman@stfc.ac.uk; alex.hannon@stfc.ac.uk

[#]Previously affiliated with Department of Physics, University of Warwick, Warwick, UK

Funding information
STFC Centre for Materials Physics and Chemistry, Grant/Award Number: CMPC09105; US National Science Foundation, Grant/Award Number: NSF-DMR 1746230

Abstract

Structures of binary PbO-SiO_2 glasses have been studied in detail over the compositional range 35 to 80 mol% PbO using high-resolution neutron diffraction, high-energy X-ray diffraction, static ^{207}Pb NMR, and structural modeling. The changes in the local environment of Pb(II) are subtle; it has a low coordination to oxygen (~3 to 4) plus a stereochemically active electron lone pair and, thus, behaves as a glass network forming (or intermediate) cation over the entire composition range. This conclusion contradicts previous reports that Pb(II) is a network modifier at low concentrations, and is supported by an analysis of lead and alkaline earth silicate glass molar volumes. The Pb-O peak bond length shortens by 0.04 Å with increasing PbO content, indicating stronger, more covalent bonding, and consistent with an increase in the number of short ($\leq$ 2.70 Å) Pb-O bonds, from 3.3 to 3.6. This is accompanied by increased axial symmetry of the Pb(II) sites, and is interpreted as a gradual transition toward square pyramidal [PbO_4] sites such as those found in crystalline PbO polymorphs. An attendant decrease in the periodicity associated with the first sharp diffraction peak (FSDP) toward that of β-PbO, accompanied by increases in the correlation lengths associated with the plumbite network (FSDP) and silicate anions (neutron prepeak), provides evidence of increased intermediate-range order and has implications for the glass forming limit imposed by crystallization. Pb(II) electron lone pairs occupy the natural voids within the silicate network at low PbO contents, while at high PbO contents they aggregate to create voids that form part of the plumbite network, analogous to the open channels in $Pb_{11}Si_3O_{17}$ and the layered structures of α- and β-PbO. Si-O and Pb-O bond lengths have been correlated with ^{29}Si and ^{207}Pb NMR chemical shifts, respectively. This is the first time that such correlations have been demonstrated for glasses and attests to the accuracy with which pulsed neutron total scattering can measure average bond lengths.

KEYWORDS
oxides, glass, silicates, structure, amorphous, lead oxide, electron lone pairs

1 | INTRODUCTION

Heavy metal, lone-pair (LP) cations, such as Tl(I), Pb(II), and Bi(III), play a unique role in the physics and chemistry of oxide glasses.[1] Heavy metal oxide (HMO) glasses are characterized by high refractive indices, nonlinear susceptibilities, and large infrared transmission windows, and hence, have wide applicability in optical devices, as well as having desirable properties for use as radiation shields and glass solders. The present contribution focuses on glasses within the PbO-SiO_2 binary, which is perhaps the most well studied of all binary HMO glass systems owing to its importance in decorative "lead crystal" glassware and ceramic glazes, its wide glass-forming range (Figure 1), as well as the ubiquitous nature of silica as a glass-forming component and the high crustal abundance of Pb.

Numerous structural studies on lead silicate glasses have been conducted using diffraction,[2–14] Pb L_{III} edge EXAFS,[15-17] ESR,[18] ^{29}Si MAS NMR,[4,19–23] ^{17}O NMR,[23] ^{207}Pb NMR,[15,21,24,25] XPS,[26–30] vibrational spectroscopy,[22,31–35] and molecular dynamics.[17,36–42] The majority of studies indicate that Pb(II) behaves as a network forming cation, with low coordination number to 3 or 4 oxygen atoms, and with a sterically active LP, at least over the range 31 to 80 mol% PbO. There is very limited evidence to suggest that the structural role of Pb(II) changes to that of a glass network modifier below ~30 mol%,[20] ~40 mol%,[27] or ~45 mol% PbO.[35] Despite this, such a structural change is often perceived as well established.

We present results from high-energy X-ray diffraction and also from neutron diffraction, where we have obtained the highest real-space resolution to date. ^{207}Pb NMR spectroscopy is used to reveal details of the subtle changes to the Pb(II) environment that occur between 35 and 80 mol% PbO, as implied by previous publications covering the evolution of the ^{207}Pb NMR lineshape between 31 and 73 mol% PbO.[15,21]

Previously, we have demonstrated[2] that the sterically active Pb(II) electron LPs in 80PbO.20SiO_2 glass organize to create voids, analogous to the channels within crystalline $Pb_{11}Si_3O_{17}$[43] and the interlayer spaces in the PbO polymorphs.[44,45] This was achieved by empirical potential structure refinement (EPSR) of neutron and X-ray diffraction data with an imposed, fixed polarization on the Pb^{2+} cations, and we here apply this technique to a low lead, 35PbO.65SiO_2, glass to reveal the probable locations of the LPs within the network, and to determine if a model consistent with Pb acting only as a network former can be derived.

We take pains to emphasize that we consider Pb(II) sites with sterically active LPs and concomitant low coordination numbers to oxygen as "network forming," consistent with the fact that oxide glasses can be obtained to very high mole fractions of PbO (Figure 1), at which, models have shown plumbite network formation,[2] indicating its role as a conditional (requiring other oxide additions) glass former. Pb(II) sites without sterically active LPs are expected to have higher coordination numbers and act like typical alkaline-earth network modifiers, with Pb(II) having a similar ionic radius to Sr(II) (see Figure 1 inset). Examples of such Pb(II) sites, with a high degree of modifier character, are found in $PbTiO_3$ perovskite,

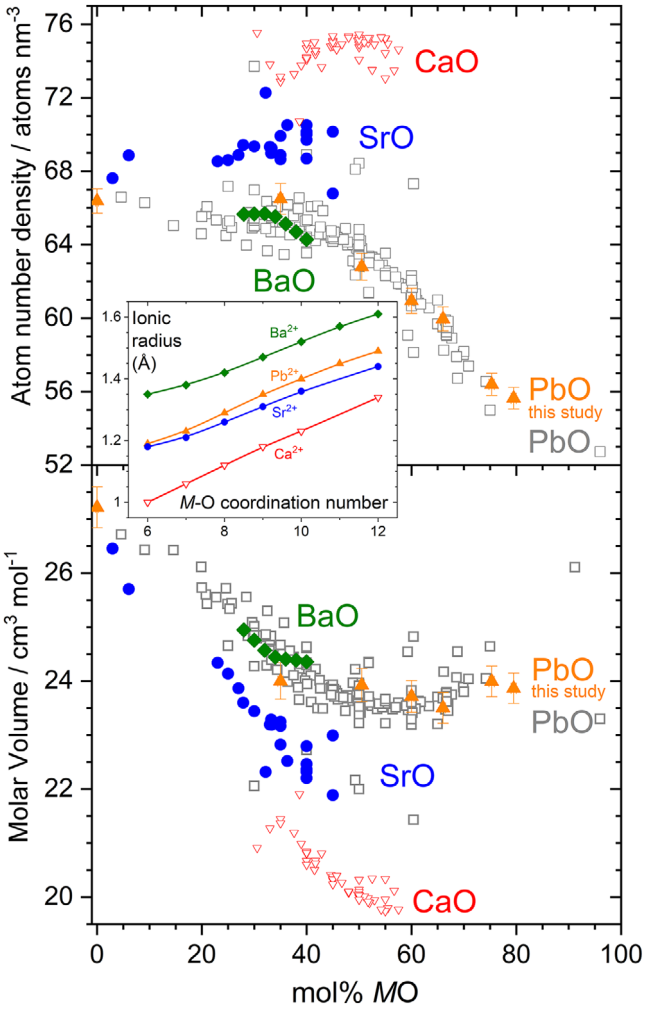

FIGURE 1 Atom number densities and molar volumes of PbO-SiO_2 glasses measured in this study (orange triangles, Table 1), compared to those of binary lead (open grey squares) and alkaline earth silicate glasses from the SciGlass database[83] (Ba - green diamonds, Sr - blue circles, Ca - red open triangles). Ionic radii are inset, plotted as a function of *M*-O coordination number.[84] It is evident that although Pb(II) has similar ion radius to Sr(II), the lead silicate glasses have smaller atom number densities and larger molar volumes than strontium silicate glasses, indicative of a different structural behavior of Pb(II) compared to Sr(II). The data also serve to illustrate the widely different glass-forming ranges for the binary silicate systems. In color online

TABLE 1 Measured molar compositions, mass and number densities, molar volumes, and glass transition temperatures for six lead silicate glasses and a silica reference

Glass composition in mol% PbO					ρ_m	ρ_0	V_M	
Nominal	Mass loss	Density	EDX	ND	g/cm^3	Atoms/nm^3	cm^3/mol	$T_g \pm 3^o$C
0.00	–	–	–	–	2.208 (22)	66.38 (67)	27.22 (38)	–
33.33	32.92 (03)	35.9 (0.8)	35.3 (6)	35.0 (5)	4.882 (49)	66.49 (84)	24.00 (34)	471
50.00	49.65 (03)	51.2 (1.1)	47.7 (4)	50.5 (5)	5.954 (60)	62.80 (73)	23.93 (31)	424
60.00	59.77 (03)	60.8 (1.3)	57.5 (4)	60.0 (5)	6.660 (67)	60.94 (68)	23.72 (29)	384
66.67	66.57 (03)	67.5 (1.4)	64.1 (2)	66.0 (5)	7.137 (71)	59.96 (66)	23.50 (29)	359
75.00	74.92 (03)	74.3 (1.6)	72.2 (4)	75.3 (5)	7.623 (76)	56.40 (60)	23.99 (28)	337
80.00	79.97 (03)	78.1 (1.6)	77.0 (6)	79.5 (5)	7.951 (80)	55.64 (59)	23.87 (28)	319

Uncertainties in parentheses. The neutron diffraction derived compositions are used in the subsequent tables.

crystalline PbB_4O_7,[46] lead borate glasses with $\lesssim$50 mol% PbO,[47,48] and lead vanadates and phosphates.[5] Furthermore, it should be noted that plumbite networks are quite distinct from canonical glass networks, such as silica, and do not follow Zachariasen's rules, owing to the low formal valence of Pb(II), and hence, relatively high oxygen-cation coordination numbers, in excess of two.

2 | MATERIALS AND METHODS

2.1 | Glass preparation

The 35–80 mol% PbO compositional range accessed in this study was limited at the lower end by the rapidly rising liquidus,[49] and at the higher end by crystallization, even under conditions of rapid twin-roller quenching.

Powders of PbO (Aldrich, 99.9+%) and SiO_2 (Aldrich, 99.6%) were mixed in quantities to yield 10 g batches of glass with nominal compositions given in Table 1. The mixtures, in pure platinum crucibles, were placed into an electric furnace for 20 min. The hold temperature of the furnace was 1000^{o}C for the three highest lead compositions, 1300^{o}C for the lowest lead composition, and 1200^{o}C for the two intermediate compositions of 50 and 60 mol% PbO. After this 20-min period, the crucibles were removed, the mass loss was recorded, and then replaced into the furnace for an additional 10 min. The glass compositions, calculated assuming mass loss due solely to volatilization of PbO, are given in Table 1. The liquids, after the second period in the furnace, were vitrified using rapid twin-roller quenching which involved pouring into a 40 μm gap between two counter-rotating steel cylinders, giving an estimated cooling rate of approximately 10^5 ^{o}C/s.[50] The resultant flakes of glass have a yellow-gold color, which is weak at low lead concentrations, but becomes very strong at 80 mol% PbO. A number of such batches were produced to obtain sufficient volume for neutron diffraction experiments. This has the disadvantage of potentially introducing small variations in glass composition and thermal history between batches, but does have the advantage of reducing the spread in glass fictive temperature which occurs as a result of the difference in thermal histories between the liquid which first contacts the roller quencher, and that which contacts last.

2.2 | Density measurement

The volumes of samples of known mass were measured by helium pycnometry in a Quantachrome Micropycnometer, and used to calculate the mass densities, ρ_m. The ρ_m obtained were used to derive molar volumes, V_M, and atomic number densities, ρ_0 (Table 1), which are plotted in Figure 1.

2.3 | Energy-dispersive X-ray spectroscopy

Glass composition was measured by using energy-dispersive X-ray spectroscopy (EDX) in a Zeiss SUPRA 55-VP field-emission gun scanning electron microscope operating at an accelerating voltage of 20 kV. Samples were mounted on aluminum stubs using an organic silver paste, and carbon coated using a vacuum evaporator to provide conduction pathways and avoid surface charging of the glass. EDX spectra were collected over 100 s exposure times at various points on the surface of a number of different glass pieces. Quantification of the glass composition was based on the integrated intensities of the Pb L and Si K lines of the spectra after background subtraction and correction for atomic number (Z) dependent electron backscatter and stopping power, absorption and fluorescence, collectively known as ZAF correction, using the EDAX Genesis software, which employs internal standards.

2.4 | Differential thermal analysis

Glass transition temperatures, T_g, were measured using a Perkin-Elmer DSC-7, and a heating rate of 40°C/min. Table 1 lists the average values extracted and most of these agree, within experimental uncertainties, with those reported by Feller et al.,[22] which were measured using the same heating rate. An exception is the 50 mol% PbO glass, for which the value in Table 1 is 41°C higher than that measured previously.[22]

2.5 | Nuclear magnetic resonance

^{207}Pb static NMR spectra were acquired using a field-step method (described previously[51]) to irradiate, with equal efficiency, the entire broad spectral envelope for Pb(II) with LP. A primary field of 7.05 T and operating frequencies of 62.36 to 62.43 MHz were used in pulse-echo ($\pi/2 \rightarrow \tau \rightarrow \pi$) experiments with $\pi/2$ and π pulse widths of 3 and 6 μs, respectively, and $\tau = 100$ μs, 2 to 8 s pulse delays, and 500 kHz spectral width at each step. A total of 960 to 1296 acquisitions were made at each of 28 or 31 steps of 22.72 kHz, resulting in total spectral widths in excess of 1.1 MHz. Spectra are referenced to tetramethyl lead at 0 ppm, using polycrystalline β-PbO as a secondary reference ($\delta_{iso} = 1515$ ppm[52]).

2.6 | Neutron diffraction

Time-of-flight neutron diffraction measurements were made using the GEM[53] diffractometer at the ISIS Neutron and Muon Source, Rutherford Appleton Laboratory, UK. The glasses, in the form of small (few mm^2) flakes, were loaded into cylindrical, thin-walled (25 μm) vanadium containers of internal diameter 8.3 mm. Data were collected with sufficient statistics to justify the use of a maximum momentum transfer $Q_{max} = 40.0$ Å^{-1} for Fourier transformation. Measurements were also performed on an empty vanadium container, the empty instrument, and an 8.34 mm diameter vanadium rod for normalization purposes and to allow for the subtraction of background signals. A vitreous silica rod was also measured.[2]

2.7 | X-ray diffraction

Wiggler beamline BW5[54,55] on the synchrotron radiation source DORIS III, HASYLAB at DESY, was used for X-ray diffraction measurements of the powdered glasses, which were held inside 1.5 mm diameter silica glass capillaries (10 μm wall thickness). Measurements of an empty capillary and the empty instrument were made to allow the removal of background scattering. The X-ray energy of 84.768 keV (wavelength $\lambda = 0.14626$ Å) was optimised so as to minimize the photoelectric absorption cross-section while avoiding fluorescence associated with the Pb K-edge at 88.0045 keV,[56] and this wavelength makes accessible a large maximum momentum transfer, $Q_{max} = 4\pi\sin(\theta_{max})/\lambda = 23.62$ Å^{-1}, at the maximum scattering angle of $2\theta_{max} = 32.0°$. Data were collected in three angular ranges using different attenuators between sample and detector, owing to the form factor dependence of the X-ray signal, and to ensure that the count rate in the Ge detector did not greatly exceed 5×10^4 counts per second. All sets of data were combined after omission of bad points, dead-time correction, normalization to the incident beam monitor counts, correction for the geometrical arrangement of the detector and sample, and scaling as required for datasets for which different levels of in-beam attenuation were used. A vitreous silica sample was also measured.[2]

2.8 | Total scattering formalism

Herein the same definitions of the real- and reciprocal-space scattering functions are used as in our previous work.[2] The real-space total correlation function is defined by

$$T^R(r) = T^{R,0}(r) + \frac{2}{\pi}\int_0^\infty Qi^R(Q)M(Q)\sin(rQ)dQ, , \quad (1)$$

where $R = N$ or X denotes the radiation type; $i^N(Q)$ is the measured distinct[57] neutron scattering, whereas

$$i^X(Q) = \frac{i(Q)}{\left(\sum_{i=1}^n c_i f_i(Q)\right)^2}, \quad (2)$$

is the measured distinct X-ray scattering after division by a sharpening[58] function used to approximately eliminate the X-ray form factor, $f_i(Q)$, Q-dependence of the scattering.[59] Subscripts i denote elements of the periodic table and c_i are atomic fractions. In Equation (1), $M(Q)$ is a modification function which can be chosen to reduce the effects of the finite limits ($0 \lesssim Q \lesssim Q_{max}$) of the integral which are used in practice. In this study, the $M(Q)$ due to Lorch[60] is chosen. The $T^{R,0}(r)$ represent average scattering density terms and are given by:

$$T^{N,0}(r) = 4\pi\rho_0 r\left(\sum_{i=1}^n c_i\bar{b}_i\right)^2, \quad (3)$$
$$T^{X,0}(r) = 4\pi\rho_0 r$$

TABLE 2 Parameters defining the interatomic pair potentials used in the structure refinements

Ion	ε, kJ/mol	σ, Å	m, (a.m.u.)	q/e
Si	2.49	0.70	28	2
O	0.92	3.16	16	−1
Pb	0.60	2.19	207	1
Pb'	0.60	2.30	103.5	1.5
LP	0.00	0.00	103.5	−0.5

The Pb' and LP parameters were used only in the lone-pair model, see main text for details.

where bound coherent neutron scattering lengths[61] are denoted $\bar{b}_i$. The $i^R(Q)$ may be written as sums of Faber–Ziman[62] partial structure factors, $S_{ij}(Q)$, and the $T^R(r)$ as sums of partial pair correlation functions, $t_{ij}(r) = 4\pi r c_j \rho_0 g_{ij}(r)$, with $g_{ij}(r)$ the standard pair distribution functions.[57,63]

2.9 | Structure refinement

The application of EPSR to the modeling of a high lead content silicate glass has been described in detail elsewhere.[2] Lead ions were modelled in two different ways, in one of which the LP of electrons was simulated by treating Pb(II) as a dipole, Pb'-LP, with separation of 1.0 Å,[64,65] which was held constant by using a large value for the intramolecular potential energy and setting the Pb' and LP masses to be equal. This is referred to as the LP model while the model without this fixed polarization applied to the Pb^{2+} ions is referred to as the Ionic model. The models for $35PbO.65SiO_2$ glass consisted of a cubic box, edge length 39.95 Å, and with the same reference potential parameters as used previously,[2] other than the $\sigma_{Pb} = 2.19$ Å and $\sigma_{Si} = 0.70$ Å (Table 2), which were adjusted slightly according to the measured average bond lengths. It should be noted that the parameters for Pb have to be modified in the presence of the LP, giving Pb'.

3 | RESULTS

3.1 | Diffraction

Data reduction procedures were conducted as described previously,[2] and the resultant interference functions, $Qi^R(Q)$, are displayed in Figure 2 (numerical data available as Supplementary Material), where, particularly in the neutron diffraction case, the importance of collecting data to high Q, with good statistics, is illustrated by the presence of oscillations extending over the full Q range. These oscillations are progressively damped as PbO replaces SiO_2. In the X-ray case, the Pb-Pb term is dominant and a clear first

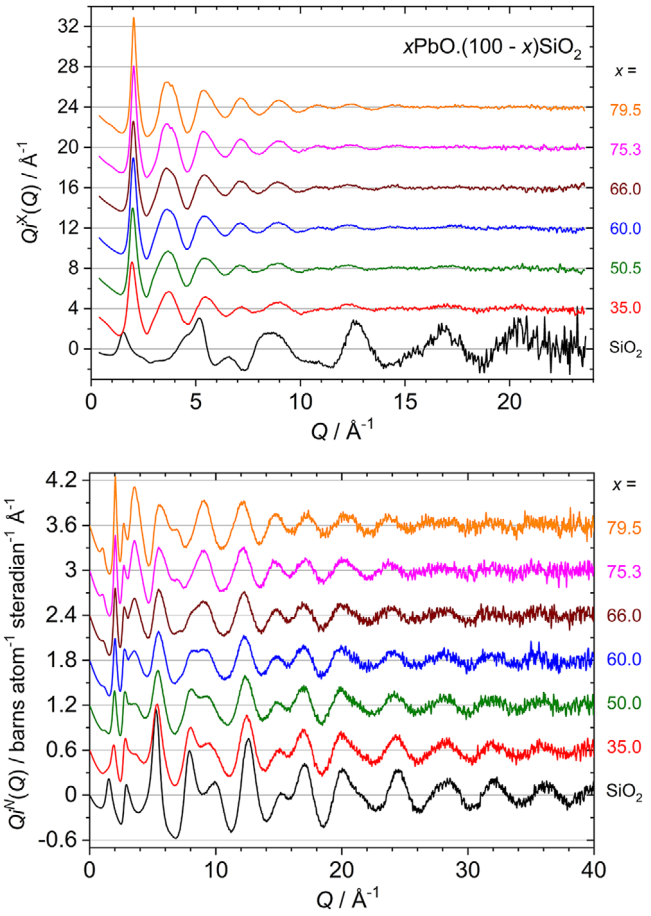

FIGURE 2 X-ray (upper) and neutron (lower) interference functions for lead silicate glasses, as compared to those measured for vitreous silica, shown to emphasize the high Q region. The mol% compositions are indicated on the plots and vertical offsets have been used for clarity

sharp diffraction peak (FSDP) at approximately 2.0 $Å^{-1}$ dominates the diffraction patterns. Figure 3 shows selected regions of the distinct scattering, $i^R(Q)$, to emphasize the low-Q features. In particular, the data for the $35PbO.65SiO_2$ glass show small-angle X-ray scattering (SAXS) intensity peaking at approximately 0.7 $Å^{-1}$. When more PbO is added to the glass composition, a prepeak, at approximately 1.2 $Å^{-1}$, becomes resolved in the neutron $i^N(Q)$ at 60 mol% PbO, and is also visible in $i^X(Q)$ for the two highest PbO content glasses. The positions and widths of the FSDPs and prepeaks are recorded in Table 3, along with their corresponding real-space periodicities and correlation lengths which are plotted in Figure 4. The real-space correlation functions obtained using $Q_{max} = 40.00$ $Å^{-1}$ (neutron) and 23.62 $Å^{-1}$ (X-ray) and Lorch[60] modification are shown in Figure 5. Compared to previous neutron diffraction studies,[3,4,6,8] the benefit of using a high Q_{max} and suitable modification function can be seen in the lower part of Figure 5, where the Pb-O peak at approximately 2.3 Å is well resolved from the O-O correlation arising from

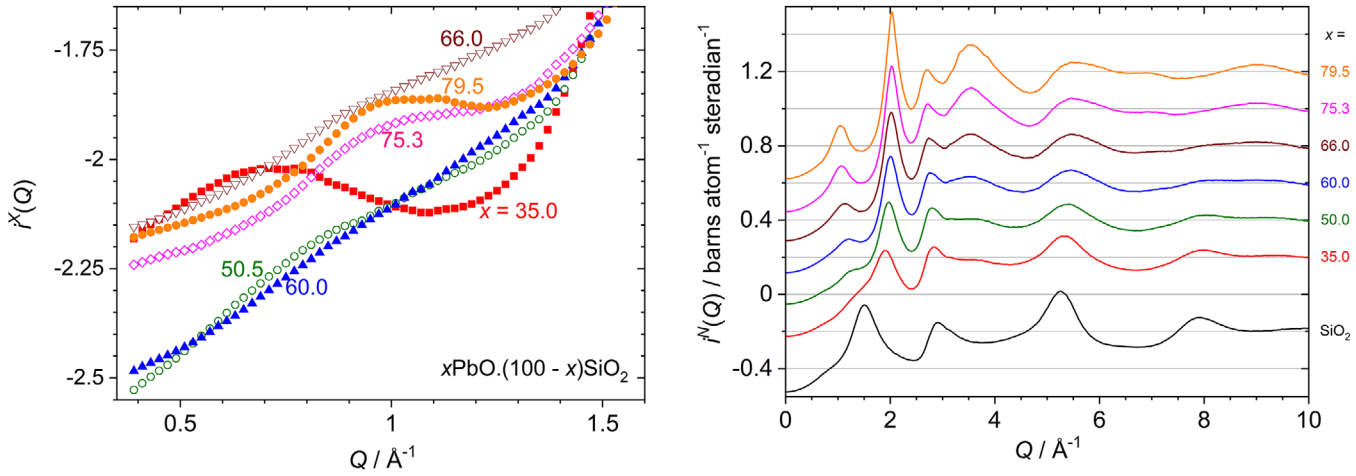

FIGURE 3 Low Q features of the X-ray (left) and neutron (right) interference functions for lead silicate glasses. The molar compositions are indicated on the plots and, in the neutron case (right) vertical offsets have been used for clarity. In color online

TABLE 3 Values obtained by fitting of Lorentzian lineshapes to the FSDPs of the X-ray and neutron distinct scattering functions, and to the prepeak of the neutron distinct scattering function

mol% PbO	Peak position Q, Å^{-1}	Peak width ΔQ, Å^{-1}	Periodicity $2\pi/Q$, Å	Correlation length $2\pi/\Delta Q$, Å	Number of periods $Q/\Delta Q$
Prepeak (ND)					
0.00	1.51 (1)	0.61 (1)	4.17 (3)	10.3 (2)	2.47 (7)
60.00	1.24 (1)	1.03 (3)	5.08 (4)	6.1 (2)	1.20 (4)
66.00	1.14 (1)	0.80 (1)	5.51 (5)	7.8 (1)	1.42 (4)
75.30	1.07 (1)	0.59 (1)	5.86 (5)	10.6 (3)	1.80 (6)
79.50	1.05 (1)	0.50 (1)	5.96 (6)	12.6 (4)	2.11 (8)
FSDP (ND)					
35.00	1.91 (1)	0.57 (2)	3.30 (2)	11.0 (4)	3.3 (1)
50.50	1.97 (1)	0.49 (1)	3.19 (2)	12.8 (3)	4.0 (1)
60.00	2.00 (1)	0.42 (1)	3.13 (2)	15.0 (4)	4.8 (1)
66.00	2.02 (1)	0.39 (1)	3.11 (2)	16.0 (4)	5.1 (2)
75.30	2.03 (1)	0.35 (1)	3.10 (2)	17.7 (5)	5.7 (2)
79.50	2.04 (1)	0.33 (1)	3.09 (2)	19.1 (6)	6.2 (2)
FSDP (XRD)					
35.00	1.94 (1)	0.52 (1)	3.24 (2)	12.1 (2)	3.7 (1)
50.50	1.98 (1)	0.43 (1)	3.18 (2)	14.6 (3)	4.6 (1)
60.00	2.00 (1)	0.39 (1)	3.14 (2)	16.1 (4)	5.1 (2)
66.00	2.01 (1)	0.37 (1)	3.13 (2)	17.1 (5)	5.5 (2)
75.30	2.03 (1)	0.34 (1)	3.10 (2)	18.4 (5)	5.9 (2)
79.50	2.04 (1)	0.32 (1)	3.09 (2)	19.7 (6)	6.4 (2)

[SiO_4] tetrahedra at approximately 2.65 Å, while truncation oscillations to either side of the peaks are practically negligible.

Sequential peak fitting to the $T^N(r)$, with appropriately broadened Gaussian bond-length distributions, was conducted as described elsewhere,[2] and is illustrated in Figure 6. The resulting parameters are recorded in Table 4 and selected average bond lengths, distribution widths, and coordination numbers are plotted in Figures 7 and 8.

3.2 | NMR

^{207}Pb static NMR spectra for selected glasses are shown in Figure 9. The chemical shift tensor components, δ_{11},

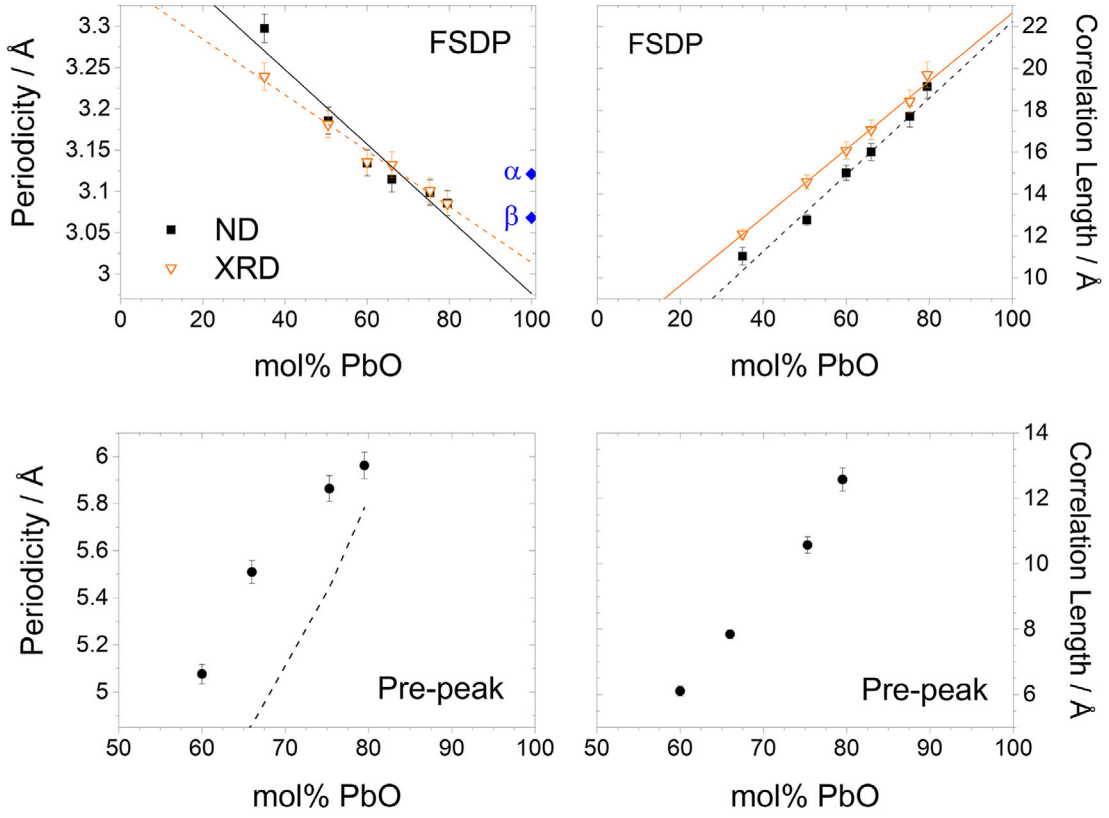

FIGURE 4 Periodicities (left) and correlation lengths (right) of the FSDP (upper), in neutron and X-ray diffraction patterns, arising from Pb-Pb separations, and of the prepeak (lower) in neutron diffraction patterns of lead silicate glasses, assigned to intersilicate anion separations. The periodicities for α-PbO (011, $d = 3.121$ Å)[45] and β-PbO (111, $d = 3.068$ Å)[44] are also shown, while, in the ideal crystalline state, the correlation lengths would be effectively infinite. Lines in the upper panels are linear fits to the data. The dashed line in the lower panel represents the average Si-Si separation, $r_{SiSi} = (c_{Si}\rho_0)^{-1/3}$, based on the partial number density $\rho_{Si} = c_{Si}\rho_0$. In color online

δ_{22}, and δ_{33}, were obtained by fitting the NMR peaks with static chemical shift anisotropy (CSA) lineshapes.[66] The peaks are then characterized by the derived CSA parameters: isotropic shift, $\delta_{iso} = (\delta_{11} + \delta_{22} + \delta_{33})/3$; span, $\Omega = \delta_{11} - \delta_{33}$; and skew, $\kappa = 3(\delta_{22} - \delta_{iso})/\Omega$; for axial symmetry $\delta_{11} = \delta_{22} \neq \delta_{33}$ and $\kappa = \pm 1$. Isotropic chemical shifts were also determined independently from any fitting by integration and determination of the first moment (center of gravity) of the spectral lineshape. In agreement with previous measurements,[15,21,23] the spectra for 35 and 50 mol% PbO silicate glasses are near identical, with only an approximately +56 ppm difference in isotropic chemical shift, compared to spans in excess of 4000 ppm (Table 5). The distribution of Pb environments in a glass means that the lineshape used in fitting should be simulated using distributions of the CSA parameters (or chemical shift tensors). Fitting with single-valued parameters, as performed herein, leads to significant uncertainties since the distributions cannot be accommodated by the broadening function which is applied to achieve a fit. This is particularly obvious for the 35 and 50 mol% PbO samples, where the lineshapes cannot adequately be approximated by any single, broadened line. Table 5 gives the parameters which have been extracted. The values of κ for the 35 and 50 mol% samples are effectively zero, indicating a range of asymmetric sites. The ^{207}Pb static NMR spectrum for 80PbO.20SiO_2 glass (Figure 9) has not previously been reported. The lineshape has a value of skew ($\kappa = 0.69$) which is approaching that of axial symmetry and strongly indicative of sites such as the square pyramidal units of α-PbO ($\kappa = 1$) and the distorted pyramidal units of β-PbO ($\kappa = 0.81$) as previously determined by Fayon et al.[52] Their values are used to simulate the lineshapes for α-PbO and β-PbO in Figure 9 for comparison.

3.3 | EPSR modeling

We have shown previously[2] that, without additional reference potential terms or constraints, EPSR[67] models of high lead silicate (80PbO.20SiO_2) glass tend to become overpolymerized with respect to the Q^n species distribution measured by ^{29}Si MAS NMR.[22] Indeed, preliminary models[68] for the six PbO-SiO_2 glasses of the present study were observed to become *progressively* overpolymerized with increasing PbO content, which is attributed to the very low weighting of the Si-Si pair term for both neutron

TABLE 4 Peak fit parameters from neutron total correlation functions from lead silicate glasses

Pair *j*-*k*	Mol% PbO	r_{jk} (Å)	$<u_{jk}^2>^{1/2}$ (Å)	n_{jk}	n_{kj}
Si-O	35.0 (5)	1.6196 (8)	0.0465 (12)	3.91 (5)	1.54 (2)
	50.5 (5)	1.6246 (6)	0.0488 (9)	3.94 (4)	1.31 (1)
	60.0 (5)	1.6294 (9)	0.0508 (13)	3.93 (6)	1.12 (1)
	66.0 (5)	1.6337 (16)	0.0545 (21)	3.98 (9)	1.01 (2)
	75.3 (5)	1.6353 (5)	0.0496 (7)	3.97 (8)	0.79 (1)
	79.5 (5)	1.6348 (23)	0.0495 (35)	3.92 (14)	0.67 (2)
Pb-O	35.0 (5)	2.2735 (3)	0.1001 (4)	2.57 (3)	0.545 (2)
	50.5 (5)	2.2829 (56)	0.1050 (2)	2.46 (2)	0.831 (2)
	60.0 (5)	2.2692 (42)	0.1000 (5)	2.38 (2)	1.018 (5)
	66.0 (5)	2.2563 (42)	0.0946 (2)	2.37 (1)	1.169 (4)
	75.3 (5)	2.2458 (13)	0.0895 (5)	2.32 (2)	1.400 (7)
	79.5 (5)	2.2300 (3)	0.0802 (3)	2.29 (1)	1.510 (5)
Pb-O	35.0 (5)	2.5015 (15)	0.0794 (13)	1.18 (2)	0.250 (3)
	50.5 (5)	2.5127 (8)	0.0692 (9)	0.86 (1)	0.289 (2)
	60.0 (5)	2.5077 (24)	0.0856 (19)	1.02 (2)	0.437 (7)
	66.0 (5)	2.5025 (14)	0.0937 (9)	1.14 (1)	0.563 (4)
	75.3 (5)	2.4598 (30)	0.0799 (25)	0.84 (2)	0.510 (10)
	79.5 (5)	2.4227 (10)	0.0705 (15)	0.85 (1)	0.562 (7)
O-O[†]	35.0 (5)	2.6447 (13)	0.07864 (95)	4.47 (11)	4.47 (11)
[SiO_4]	50.5 (5)	2.6529 (10)	0.07864 (95)	3.82 (8)	3.82 (8)
	60.0 (5)	2.6608 (15)	0.07864 (95)	3.27 (8)	3.27 (8)
	66.0 (5)	2.6679 (25)	0.07864 (95)	2.95 (10)	2.95 (10)
	75.3 (5)	2.6704 (8)	0.07864 (95)	2.30 (5)	2.30 (5)
	79.5 (5)	2.6695 (38)	0.07864 (95)	1.95 (9)	1.95 (9)
Pb-O	35.0 (5)	–	–	3.75 (4)	0.795 (3)
Total	50.5 (5)	–	–	3.32 (2)	1.120 (3)
	60.0 (5)	–	–	3.40 (3)	1.456 (9)
	66.0 (5)	–	–	3.52 (2)	1.733 (6)
	75.3 (5)	–	–	3.16 (2)	1.910 (13)
	79.5 (5)	–	–	3.14 (2)	2.071 (9)
O-X Sum	35.0 (5)	–	–	2.33 (2)	–
(X = Pb,Si)	50.5 (5)	–	–	2.43 (1)	–
	60.0 (5)	–	–	2.58 (2)	–
	66.0 (5)	–	–	2.74 (2)	–
	75.3 (5)	–	–	2.70 (1)	–
	79.5 (5)	–	–	2.74 (2)	–

[†]Parameters fixed at those predicted from Si-O peak area and position and assumption of tetrahedral geometry. Width fixed at that measured for vitreous silica. Statistical uncertainties in parentheses.

and X-ray scattering. However, when the PbO content is low enough, as for the 35PbO.65SiO_2 glass, quantitative agreement between Q^n species distributions from the model and ^{29}Si NMR is found.[68] Therefore, we focus here on the modeling of the 35 mol% PbO silicate glass, such that the gross structural differences, and similarities, with previously published[2] models of an 80 mol% PbO silicate glass can be enumerated and discussed.

Table 6 lists some ensemble (>6.8 × 10^3 configurations) average values derived from EPSR models of 35PbO.65SiO_2 glass, both with (LP) and without (Ionic) the fixed polarization applied to the Pb^{2+} ions. A snapshot of the LP model is illustrated in Figure 10, while the model interference functions, $Qi^R(Q)$, are compared to those measured by neutron and X-ray diffraction in Figure 11. Also shown (Figure 11) are the weighted partial pair interference functions which

TABLE 5 ^{207}Pb NMR peak fit parameters

mol% PbO	δ_{11} (ppm)	δ_{22} (ppm)	δ_{33} (ppm)	$\delta_{iso} = (\delta_{11}+\delta_{22}+\delta_{33})/3$ (ppm)	δ_{iso} from 1st moment (ppm)	$\Omega = \delta_{11} - \delta_{33}$ (ppm)	$\kappa = 3(\delta_{22}-\delta_{iso})/\Omega$
35	2110	35	−1990	50	80	4110	−0.01
50	2110	70	−1950	80	130	4060	0.00
80	2570	1925	−1650	950	880	4220	0.69
β-PbO	3165	2550	−1780	1310	1210	5020	0.75

Chemical shift components in ppm with respect to tetramethyl lead. Also shown are the first moment "center-of-gravity" values for isotropic chemical shift, obtained by integration of the experimental spectra. Uncertainties are approximately ±100 ppm.

TABLE 6 Details of EPSR models for 35PbO.65SiO_2 and 80PbO.20SiO_2 glasses

Parameter	35 mol% PbO Models		80 mol% PbO Lone-Pair Q^0 model[2]
	Ionic	Lone-pair	
R-factor (× 10^3)[67]	1.43	1.60	1.82
Total energy, kJ/mol	−730.2	−792.6	−572.6
Mean O-Si-O angle	109.3	109.4	109.8
RMS deviation	6.0	5.8	5.1
Mean Si-O-Si angle	143.1	144.6	167.5
RMS deviation	16.5	16.5	6.7
Mean Pb-O-Pb angle	106.5	108.5	109.7
RMS deviation	13.4	13.2	14.4
Mean Si-O-Pb angle	127.7	128.0	124.1
RMS deviation	16.4	16.9	16.2

Only short (≤2.7 Å) Pb-O bonds have been considered in the calculations of mean bond angles. See Alderman et al.[2] For further details of 80PbO.20SiO2 glass models.

show clearly the dominant contributions to the experimental neutron (O-O, Si-O) and X-ray (Pb-X) diffraction patterns. It is evident that the two models, Ionic and LP, are substantially the same at this composition, as far as the goodness-of-fit and partial structure factors are concerned.

Real-space pair correlation functions, $g_{ij}(r)$, are plotted in Figure 12, where it is clear that the Pb-O peak has a shoulder to the high r side, and $g_{PbO}(r)$ does not fall to zero after its first maximum. As such, Table 7, which records various coordination number distributions (CNDs), shows those for two characteristic Pb-O cut-off radii of $r_2 = 2.70$ or 3.27 Å. Figure 13 compares the $g_{LPLP}(r)$ of 35 and 80 mol% PbO^2 silicate glasses. Selected bond angle distributions (BADs) are displayed in Figure 14 and Table 6 records some of their mean values and standard deviations.

4 | DISCUSSION

4.1 | Local environment of Pb(II)

A key conclusion of the present study is that the first coordination sphere, and hence structural role, of Pb(II) changes little with lead silicate glass composition, at least over the range 35 to 80 mol% PbO. The diffraction and modeling results show that Pb-O coordination numbers are low (~3 to 4) over the entire range, and therefore, PbO acts as a glass network forming (or intermediate) oxide, with a stereochemically active electron LP on each Pb(II). This is supported by ^{207}Pb NMR spectroscopy, the positive values of isotropic shift (Table 5) being typical of more covalently bonded Pb(II).[52] This relatively unchanging role contradicts current perception,[27,35] which proposes compositions below which the role of Pb(II) is that of a network modifier. Although a change at al.[20]) less than those discussed here cannot be ruled out, we argue that this is unlikely because of the invariant tetrahedral coordination of silicon by oxygen. This can be made clear by contrasting with the binary PbO-B_2O_3 glasses where both diffraction[47,69] and ^{207}Pb NMR[24,48,70] clearly do show evidence of a change in Pb-O coordination and structural role; however, this is accompanied by a change in boron-oxygen coordination number. The conversion of [BO_3] to [BO_4]$^-$ means that nonbridging oxygen (NBO) atoms do not form at low PbO loadings, and the bridging oxygen (BO) atoms present can only, based on electrostatic bond strength sums, form comparatively weak, long, and more ionic Pb-O bonds. In the PbO-SiO_2 glasses, no change

TABLE 7 Average coordination numbers and coordination number distributions (CNDs), expressed as percentages, for various atom pairs in the EPSR models of the $35PbO.65SiO_2$ glass

Atom pair (r_2, Å)	System	Coordination number							Average N'_{ij}
		0	1	2	3	4	5	6	
Si-O (2.0)	Ionic	0	0	0	0.6 (1)	99.4 (3)	*0*	0	3.99 (8)
	Lone-pair	0	0	0	0.4 (1)	99.6 (2)	*0*	0	4.00 (7)
O-Si (2.0)	Ionic	2.05 (3)	38.9 (2)	58.7 (2)	0.33 (4)	0	0	0	1.57 (54)
	Lone-pair	3.02 (3)	37.08 (0)	59.38 (1)	0.52 (4)	0	0	0	1.57 (56)
	^{29}Si MAS NMR	-1 (11)	41.6 (7.0)	59.2 (3.9)	0	0	0	0	1.60 (47)
Si-Si (3.48)	Ionic	0.20 (2)	3.54 (0)	18.2 (2)	48.3 (3)	28.8 (4)	1.0 (2)	*0*	3.05 (82)
	Lone-pair	*0*	2.5 (1)	18.8 (2)	45.0 (3)	31.8 (3)	1.8 (2)	*0*	3.12 (82)
	^{29}Si MAS NMR	1 (3)	5 (3)	21 (3)	42 (3)	30 (3)	0	0	2.93 (67)
Pb-O (2.7)	Ionic	*0*	0.9 (3)	13.0 (1.0)	43.3 (1.5)	37.5 (1.4)	5.2 (7)	0.2 (1)	3.33 (81)
	Lone-pair	*0*	0.2 (2)	11.0 (9)	48.3 (1.5)	35.7 (1.3)	4.8 (6)	0.05 (9)	3.34 (74)
O-Pb (2.7)	Ionic	53.7 (3)	25.3 (5)	18.3 (3)	1.8 (1)	0.84 (6)	*0*	0	0.71 (88)
	Lone-pair	54.5 (3)	24.4 (4)	17.8 (3)	2.4 (1)	0.93 (0)	*0*	0	0.71 (90)
Pb-O (3.27)	Ionic	0	*0*	0.5 (2)	8.9 (9)	38.6 (1.7)	35.9 (1.8)	13.9 (1.2)	4.61 (94)
	Lone-pair	0	0	0.3 (2)	9.4 (8)	35.1 (1.5)	37.7 (1.7)	14.6 (1.2)	4.66 (96)
O-Pb (3.27)	Ionic	39.6 (4)	30.9 (5)	22.9 (4)	5.4 (3)	1.1 (1)	0.04 (3)	*0*	0.98 (97)
	Lone-pair	39.2 (4)	30.7 (5)	23.6 (3)	5.0 (2)	1.4 (1)	0.07 (3)	0	0.99 (98)

Standard deviations are shown in parentheses—in the final column these represent the widths of the coordination number distributions. The *Q* species distribution for a $33.3PbO.66.7SiO_2$ glass, measured by ^{29}Si MAS NMR,[22] has been used to estimate the Si-Si and O-Si CNDs, shown for comparison. The upper cut-off radius, r_2, is given in the first column. Values smaller than 0.01% are expressed as italicized zeros. A few percent of Pb are coordinated to seven O for $r_2 = 3.27$ Å.

in Si-O coordination has been observed, nor is expected (at ambient pressure) at lower PbO contents ($\lesssim$ 35 mol% PbO), and therefore, NBOs must be present, to which strong, short, and more covalent Pb-O bonds *can* form.

The following discussion covers those aspects of the Pb(II) environment which *do* change over the 35 to 80 mol% PbO range. Most striking is the change in ^{207}Pb NMR lineshape (Figure 9), and values of skew indicating an increase in axial symmetry of the Pb^{2+} site with increasing PbO content. Indeed there is great similarity between the measured spectra for $80PbO.20SiO_2$ glass and β-PbO, although the glass spectrum has an isotropic shift (δ_{iso}) approximately 400 ppm less positive than that of the crystal. Changes in the ^{207}Pb NMR spectra as PbO content increases are accompanied by small, but significant, changes in the Pb-O pair correlations measured by diffraction. These include: (i) a reduction in the *peak* Pb-O bond length (Figure 6), (ii) a reduction in width of the first fitted Pb-O peak (Figure 6), (iii) changes in the shape of $g_{PbO}(r)$ (Figure 12), (iv) changes in O-Pb-O BAD (Figure 14).

The Pb-O environment is difficult to characterize unambiguously due to the asymmetry (shoulder to high *r*) of the Pb-O bond length distributions (Figures 4, 5, 11) and the overlap between first and second shell Pb-O distances, giving rise to a nonzero minimum in $g_{PbO}(r)$ at distances greater than the first peak maximum (Figure 12). In calculating the Pb-O coordination numbers, and their distributions, from EPSR models (Table 7) we have, therefore, chosen two different radial cut-offs, r_2, of 2.70 and 3.27 Å, to include only "short" and "short" plus "long" Pb-O bonds, respectively. Comparing the values obtained for $35PbO.65SiO_2$ glass (Table 7) with our previously published results for $80PbO.20SiO_2$ glass,[2] it is evident that there is a small increase, of approximately 0.2, in the average number of short Pb-O bonds from 3.33 at 35 mol% PbO, to 3.55 at 80 mol% PbO. This is consistent with a transition toward a more axially symmetric, square pyramidal environment, at higher PbO content, as implied by the ^{207}Pb NMR results. There is much greater experimental uncertainty regarding the number of longer Pb-O bonds, however, modeling indicates there are approximately 1.3 longer Pb-O bonds at 35 mol% PbO and 1.1 to 1.5 at 80 mol% PbO, dependent upon model specifics.[2] Note that the above values are not directly comparable with those from peak fitting (Table 4, Figures 6 and 7), where the *effective* cut-off radius tended to decrease as PbO content increased, due to decreasing peak positions and widths.

The O-Pb-O BAD (Figure 14) shows an increase in local order at high PbO contents, and this is also consistent with ^{207}Pb NMR results, and the small increase, of approximately 0.2, in the average number of short Pb-O bonds. As discussed previously,[2] the O-Pb-O BADs derived by EPSR

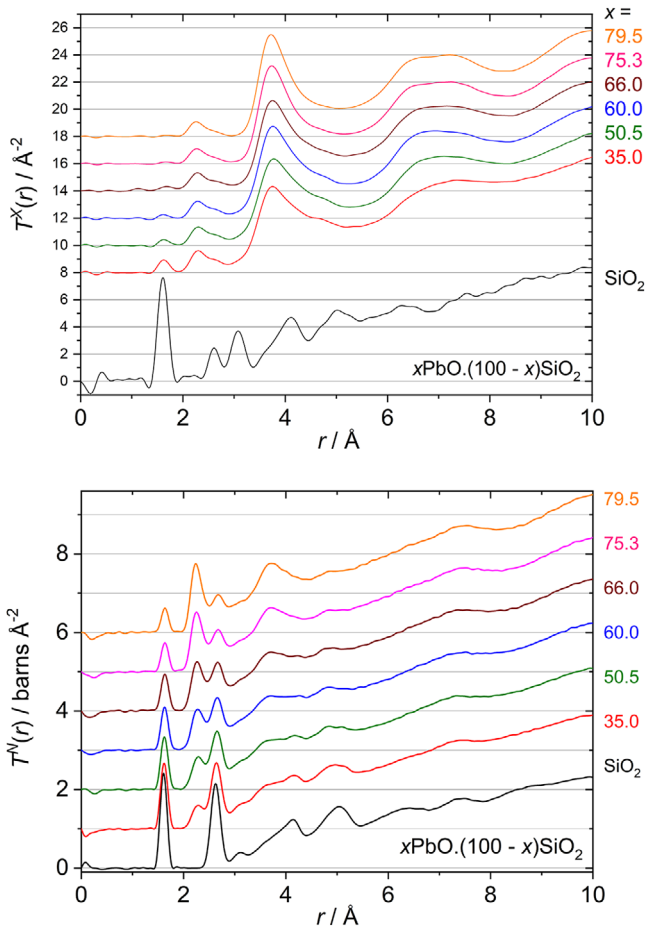

FIGURE 5 Total X-ray (upper) and neutron (lower) correlation functions from lead silicate glasses, as compared to that measured for vitreous silica. A Lorch[60] modification function and $Q_{max} = 23.62$ Å^{-1} (X-ray) or 40.00 Å^{-1} (neutron) were used. Vertical offsets have been used for clarity

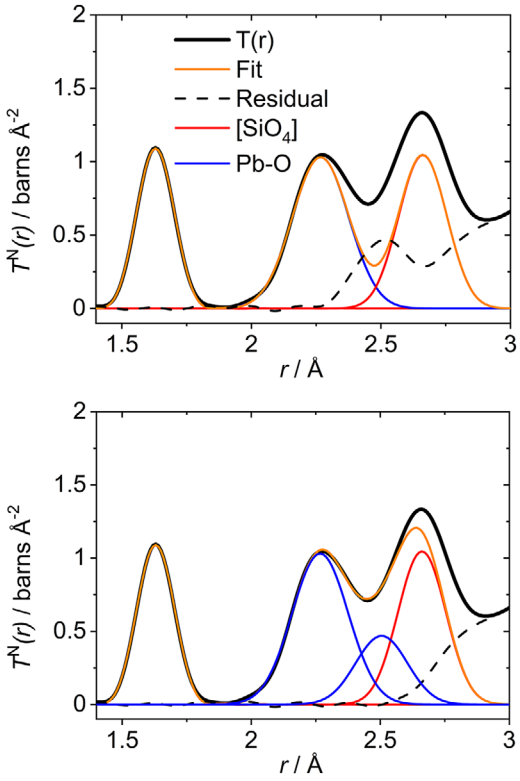

FIGURE 6 Example peak fits to the neutron total correlation function for 60PbO.40SiO_2 glass. The upper panel shows the result after fitting the Si-O peak (~1.6 Å) and the leading edge of the Pb-O feature (~2.25 Å), and includes the predicted O-O correlation arising from [SiO_4] tetrahedra (~2.65 Å). There is a clear peak in the residual at approximately 2.5 Å. The lower panel shows the final result after fitting to the peak in the residual (attributed to longer Pb-O bonds) and allowing the two Pb-O peaks to adjust while keeping other peaks fixed. In color online

also show greater local order than those derived by RMC methods,[3] and this is true over the full range of glass compositions. Indeed, at 80 mol% PbO, the EPSR -derived O-Pb-O BAD approaches that of crystalline $Pb_{11}Si_3O_{17}$,[43] as well as those of the PbO polymorphs, demonstrating that it generates a more realistic picture than the broader, RMC-derived BADs.

The decrease of r_{PbO} and the narrowing of the first Pb-O peak fitted to $T^N(r)$, with increasing PbO content (Figure 7), are evidence for strengthening and an increased covalency of these bonds. This is consistent with the measured change in position of the ^{207}Pb NMR spectrum with glass composition. Figure 15 shows the chemical shift of the ^{207}Pb NMR lineshape (center of gravity) as a function of the *peak* bond length measured by diffraction. Results for some lead germanate glasses[71] have been included to increase the significance of the linear correlation, where a least-squares fit yields (in ppm and Å):

$$\delta_{iso}\left(^{207}Pb\right) = (-1.32\,(26)\,r_{PbO}\,(\text{peak}) + 3.04\,(59)) \times 10^4 \quad (R = -0.916 \text{ for } N = 7). \tag{4}$$

This is the first time that parameters measured by ^{207}Pb NMR and diffraction have been correlated for *a series of glasses*. The above result is similar to that determined by Fayon et al.,[52] ($\delta_{iso}(^{207}Pb) = -8668.95\ r_{PbO} + 20854$) for a range of crystalline materials. The offset, of approximately 0.1 Å, between the two trends arises from our use of peak (most common) bond length, as opposed to mean bond length, and is consistent with the observed existence of additional, longer, Pb-O bonds in the glasses (i.e., average bond length > peak bond length). Note that the range of Pb-O bond lengths covered here (0.08 Å) is very much smaller than that covered by Fayon et al.[52] (0.66 Å) in their study of crystalline materials which showed a large degree of scatter in the short r_{PbO} region. Thus, while the

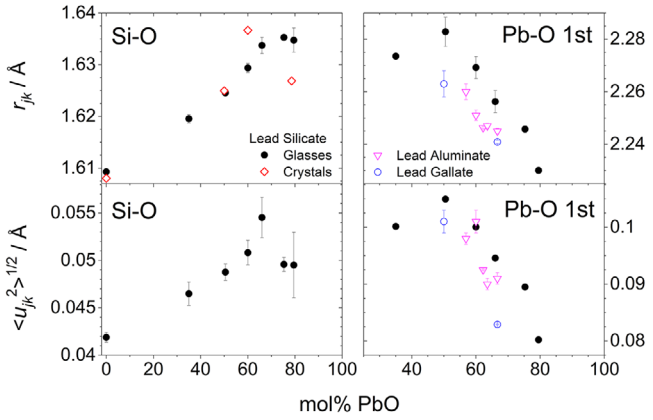

FIGURE 7 Mean lengths, r_{jk}, and widths, $< u_{jk}^2 >^{1/2}$, for Si-O and short Pb-O bond length distributions, from fits to neutron total correlation functions from lead silicate glasses (filled circles). Numerical values are listed in Table 4. The open diamonds represent the average Si-O bond lengths in quartz[72] and lead silicate crystals.[43,73,74,75] Note that in Pb_2SiO_4,[73] $r_{SiO} = 1.6601$ Å is unusually large, and is not within the range of the plot. Equivalent Pb-O parameters for PbO-$AlO_{1.5}$ aluminate[85] and PbO-$GaO_{1.5}$ gallate[86,87] glasses are shown for comparison

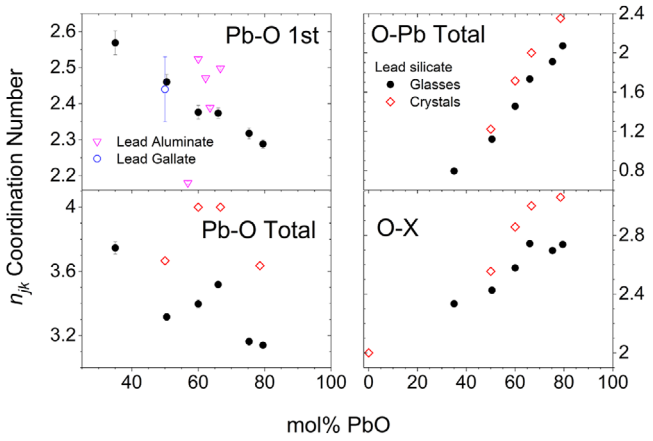

FIGURE 8 Coordination numbers from fits to neutron total correlation functions from lead silicate glasses. The numbers $n_{OX} = n_{OPb} + n_{OSi}$. Absolute values are listed in Table 4. The open diamonds represent the average coordination numbers in quartz[72] and lead silicate crystals,[43,73,74,75] where cut-offs of 2.7 and 2.0 Å have been chosen for Pb-O and Si-O bonds, respectively. Equivalent Pb-O parameters for PbO-$AlO_{1.5}$ aluminate[85] and PbO-$GaO_{1.5}$ gallate[86,87] glasses are shown for comparison

present results reveal that a correlation between $\delta_{iso}(^{207}Pb)$ and r_{PbO} also holds for the more covalent materials, this, combined with the published observations for crystals, would imply significant dependence on the second oxide component. Indeed, Figure 15 indicates that improved correlations would be obtained by fitting the data for silicate and germanate glasses separately, although the number of data points in each case is too low to do so with confidence.

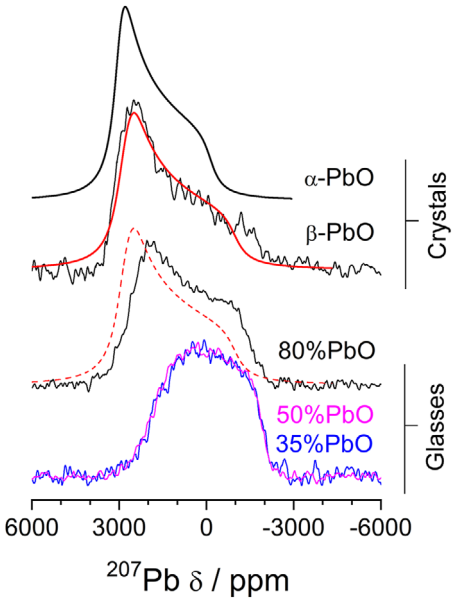

FIGURE 9 ^{207}Pb static NMR spectra for three lead silicate glasses and for β-PbO. Suitably broadened simulations of the static CSA lineshapes for polycrystalline α- and β-PbO (overlaid on the measured spectra for the crystal and 80 mol% PbO glass (dashed line)), based on parameters reported by Fayon et al.,[52] are shown for comparison. The slight excess intensity near −1500 ppm in the experimental spectrum from β-PbO is due to the presence of some basic lead carbonate impurity in the sample. Vertical offsets have been applied for clarity, in color online

4.2 | Si-O bond lengths

From Figure 7 it is apparent that the Si-O bond lengthens significantly with increasing PbO content. A similar effect is apparent when comparing bond lengths in quartz[72] and lead silicate crystals[43,73–75] (Figure 7). The size of the effect can also be compared to the thermal expansion of the Si-O bond, with an equivalent $\Delta T \simeq 3200$ K ($\Delta x \simeq 80$ mol% PbO), using the linear thermal expansion coefficient ($\alpha_{Si\text{-}O} = 5.0(6) \times 10^{-6}$ K^{-1}) reported by Dove et al.[76] for β-cristobalite.

We are not aware of previous reports of any set of Si-O bond lengths with such high precision for any binary silicate glass series. We therefore take the opportunity to discuss some of the structural implications of the observed trend. It has been demonstrated[77,78] that the Si-O-Si bond angle and Si-O bond length are correlated, with the latter increasing as the former decreases, and the oxygen p-orbital character increases. Thus, one might naively interpret the trend in Figure 7 as indicating that an increase in PbO leads to a reduction in Si-O-Si angle. However, it also results in depolymerization of the silicate network resulting in Si-O-Pb linkages. There are then two additional effects to consider: (i) the number of Pb coordinating

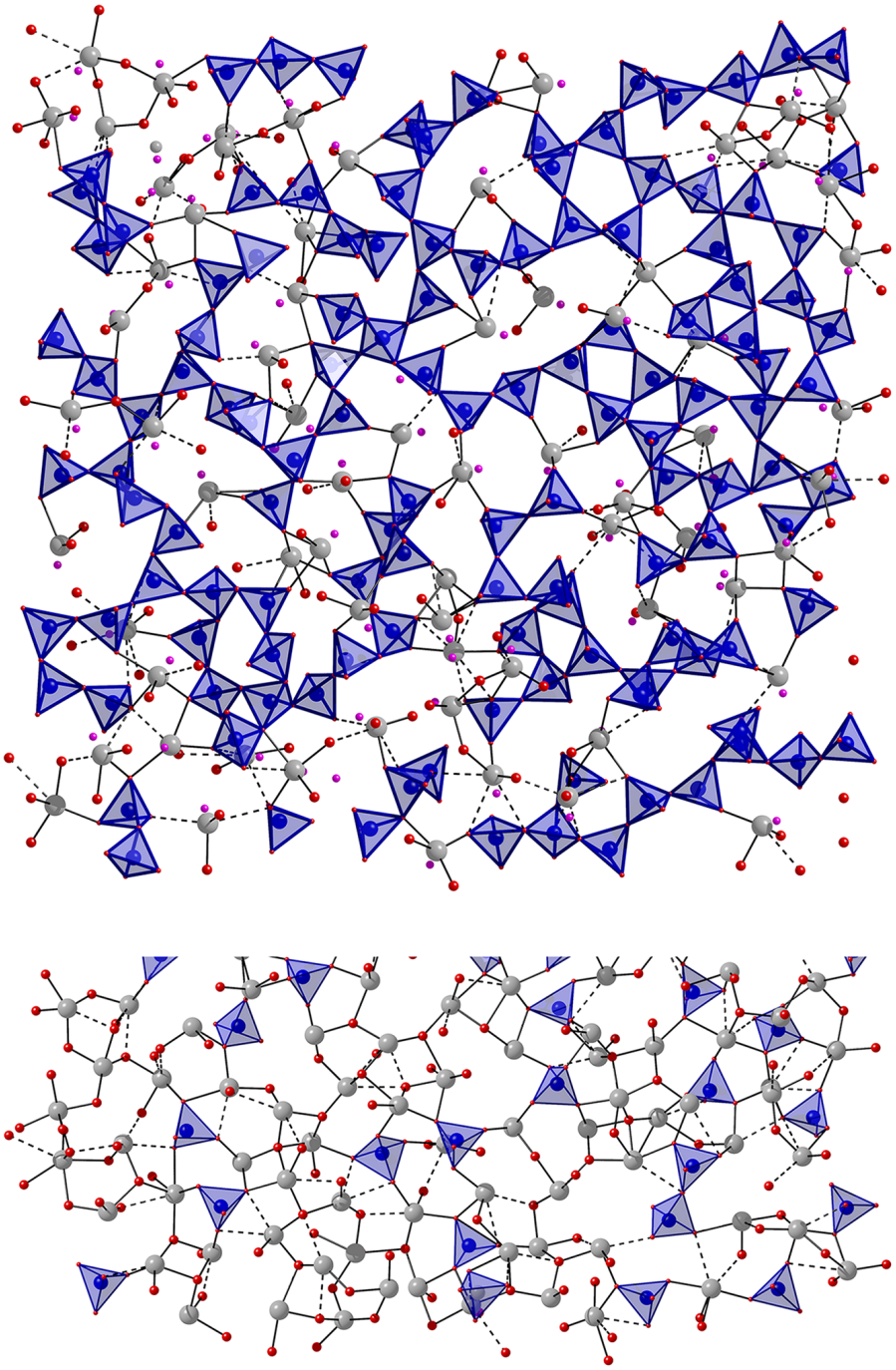

FIGURE 10 Slices, ~5 Å thick, through single configurations of EPSR models of $35PbO.65SiO_2$ (upper) and $80PbO.20SiO_2$[2] (lower) glasses. The areas shown are 40×40 Å^2 (upper) and 43×19 Å^2 (lower) and correspond to the LP and LP Q^0 models, respectively. Si atoms are shown within shaded (blue) tetrahedra, Pb atoms as large (grey) spheres, bonded to O atoms (smaller spheres, red). Pb-O bonds shorter than 2.7 Å are shown as solid lines, while those between 2.7 and 3.27 Å are dashed. LPs are shown as pink spheres, but have been omitted from the lower image for clarity. The Si and Pb coordination spheres have been completed, whereas the O ones have not. In color online

to a NBO; (ii) the Si-O-Pb bond angles. The fact that the NBO-Pb coordination number increases with PbO content can be inferred by comparing the CNDs in Table 7, for the $35PbO.65SiO_2$ glass, to those previously published[2] for $80PbO.20SiO_2$ glass. Such an increase in the number of coordinating Pb should itself cause an elongation of the Si-O bonds. This effect is further compounded by the decrease in the average Si-O-Pb bond angle (Table 6, Figure 14) as PbO is added to the glass composition. This latter contribution is not entirely independent, and is thought to be due to the steric repulsion between Pb pairs due to the increasing average NBO-Pb coordination number.

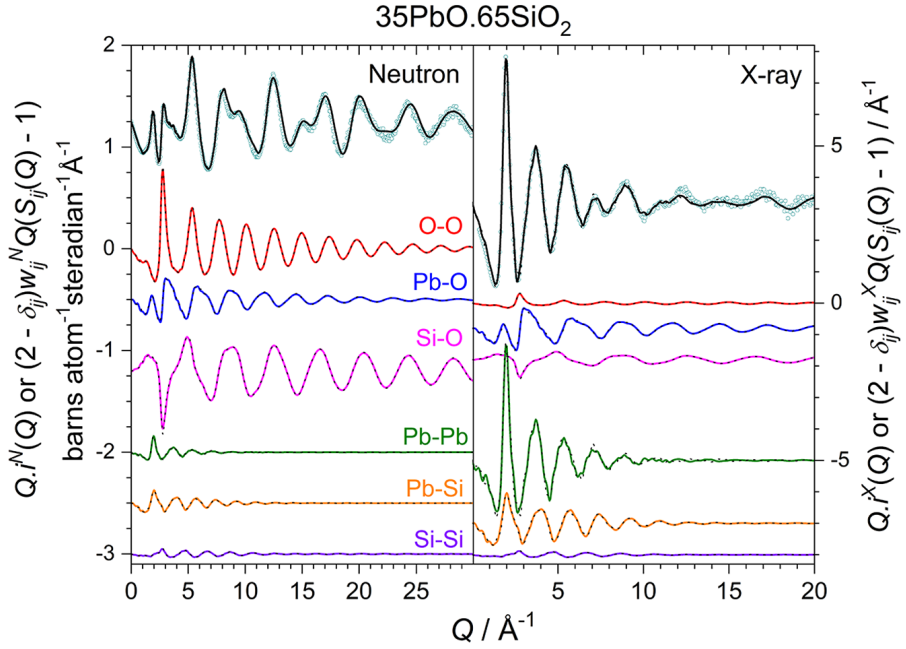

FIGURE 11 Interference functions measured (open circles) by neutron (left) and X-ray (right) diffraction for the 35PbO.65SiO_2 glass, compared with model functions. The appropriately weighted partial pair interference functions are shown vertically offset for clarity, in the same order in both panels. Ionic model: thick lines (various colors), lone-pair model: thin dotted lines (black). In color online

Following the linear increase of r_{SiO} with PbO content, there is a plateau in r_{SiO} between approximately 67 and 80 mol% PbO (Figure 7). This is likely indicative of the growing dominance of monomeric, Q^0, and dimeric, Q^1, species, as measured by ^{29}Si MAS NMR,[22] where the large Si-O-Si bond angles typical of the Q^1 dimers are associated with a contraction of the average Si-BO bond.

Both the Si-O bond length and the Si-O-Si bond angle have previously been correlated with the isotropic ^{29}Si NMR chemical shift, δ_{iso}, for various silicate minerals and zeolites, as reviewed by Mackenzie and Smith.[79] Here, for the first time, we are able to demonstrate a correlation between measured average Si-O bond length, and average (first moment) ^{29}Si MAS NMR chemical shift[22] in *a series of glasses*. This is illustrated in Figure 15, where the linear fit, given by (in ppm and Å)

$$\delta\left(^{29}\mathrm{Si}\right) = (1.255\,(91)\,r_{SiO} - 2.13\,(15)) \times 10^3$$
$$(R = 0.987 \text{ for } N = 7)\,, \qquad (5)$$

is close, over the region studied, to the composite trend given by MacKenzie and Smith[79] as $\delta = 999\ r_{SiO} - 1709$.

Also shown in Figure 7 are the widths, $< u_{SiO}{}^2 >^{1/2}$, which pass through a maximum at approximately 67 mol% PbO, which reflects the Q^n species distribution, whose standard deviation itself passes through a maximum at approximately 50 mol% PbO. The difference in location of these two maxima indicates additional broadening mechanisms of the Si-O bond length distribution, which are the distribution of different O-Pb coordination numbers and the local structural disorder about the Pb atoms. In other words, the reduction in $< u_{SiO}{}^2 >^{1/2}$ with PbO content above approximately 67 mol% PbO is attributed to a narrowing of the oxygen site distribution, due to both the Q^n species and Pb site distributions also narrowing.

4.3 | Oxygen environments

In contrast to the cationic environments, the anionic environments change drastically with lead silicate glass composition. This can be viewed as a continuous transition from the [OSi_2] BO environments, with less *p* character, in SiO_2 glass, toward the distorted sp^3 hybridized [OPb_4] plumbite oxygen environments common to the PbO polymorphs and lead silicate crystal structures. Our EPSR models which are in best agreement with the silicate *Q*-speciations derived from ^{29}Si MAS NMR indicate 2–3% plumbite (or "free") oxygen at 35 mol% PbO (Table 7) and 35% at 80 mol% PbO.[2] These amounts are in reasonably good agreement with the 2 and 40%, respectively, predicted based on the equilibrium constant of $K \approx 12$ for the reaction 2(Pb-O-Si) → Pb-O-Pb + Si-O-Si, as derived from O 1s X-ray photoelectron spectroscopy measurements.[30] The oxygen speciations in our models also compare favorably with a similar analysis based on ^{17}O NMR spectroscopic measurements on lead silicate glasses.[23]

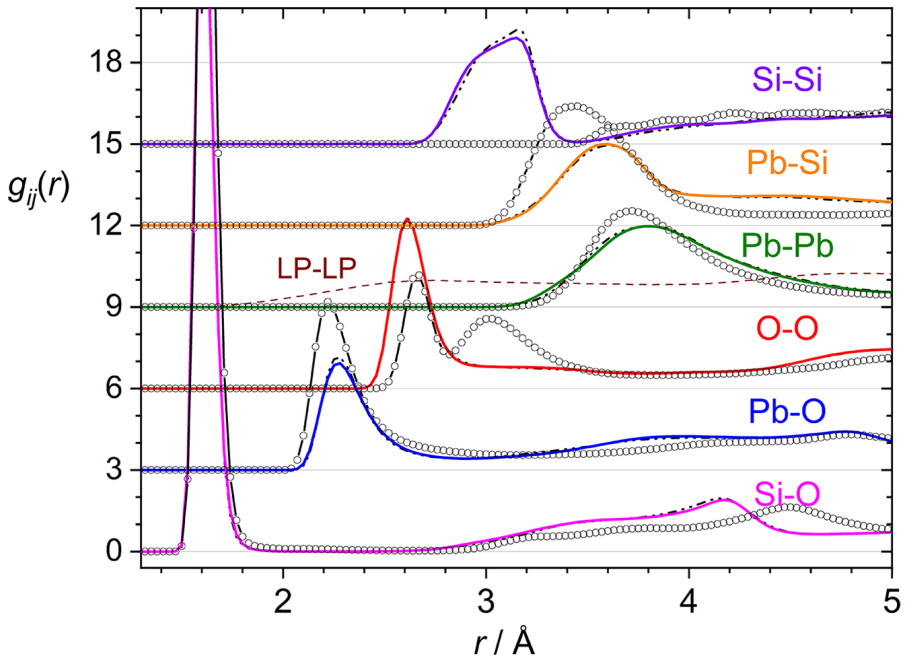

FIGURE 12 Model partial pair correlation functions for the $35PbO.65SiO_2$ glass. Vertical offsets have been used for clarity. The LP-LP and Pb-Pb functions are shown on an enlarged scale in Figure 13. Ionic model: thick lines (various colors), lone-pair model: thin dotted lines (black). The $g_{ij}(r)$ for the depolymerized ("Q^0") LP model of $80PbO.20SiO_2$ glass[2] are shown for comparison as open circles with a connecting line. In color online

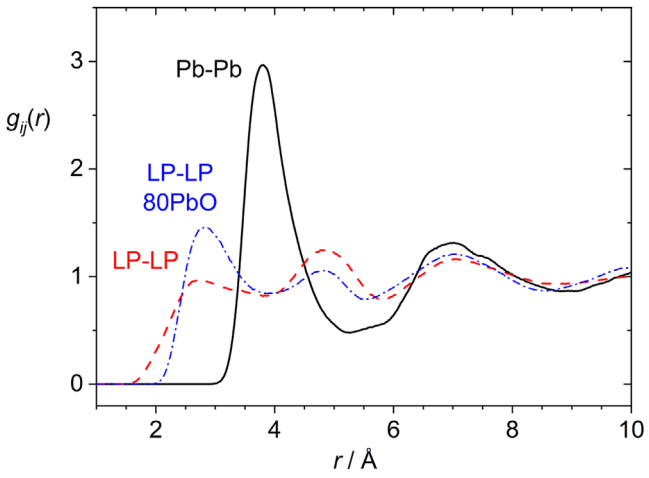

FIGURE 13 LP-LP partial pair correlation function for the $35PbO.65SiO_2$ glass compared to the Pb-Pb function from the same model, and the LP-LP function from the depolymerized ("Q^0") LP model of $80PbO.20SiO_2$ glass[2]

4.4 | Pb lone pair distributions and intermediate-range order

The emergence of voids within high lead silicate glasses, owing to the organization of electron LPs, constitutes a key insight, made possible by the use of empirical structural modeling using polarized Pb^{2+} ions.[2] Such voids in high lead (80 mol% PbO) silicate glass are analogous to the open channels in $Pb_{11}Si_3O_{17}$ and the layered structures of α- and β-PbO, and are characteristic of the plumbite glass network. At lower PbO contents, there is less tendency for LPs to cluster within voids, as is evident from Figures 10 and 13, and rather the Pb^{2+} LP electron density occupies voids within the *silicate* network (see Figure 10), which are present as a result of the restricted Si-O-Si BAD and resultant topological constraints. The sharpening of the FSDP (attributed to Pb-Pb separations) with increasing PbO content (Figures 1 and 4) is considered to be a consequence of the ordering of LPs within voids, and resultant *local* layer-like structures, which form as the plumbite network regions increase in size, up to approximately 20 Å (Figure 4, Table 3). The concomitant reduction in periodicity associated with the FSDP position (Figure 4) likely has consequences for the glass formation limit, as it, along with the local structure about the Pb atoms, becomes similar to that of β-PbO.

Edge-sharing of contiguous $[PbO_m]$ polyhedra is another hallmark of plumbite glass networks and probably prevents glass-formation above 83 mol% PbO.[2,22] However, it is worth noting that the edge-sharing $[Pb_2O_4]$ pairs of trigonal pyramids proposed by Takaishi et al.[4] as the basic motif of the plumbite network over the entire compositional range is potentially misleading. The unit was proposed on the basis of the nearest neighbor Pb-Pb separation in $T^X(r)$ being independent of glass composition. However, within our structural models,

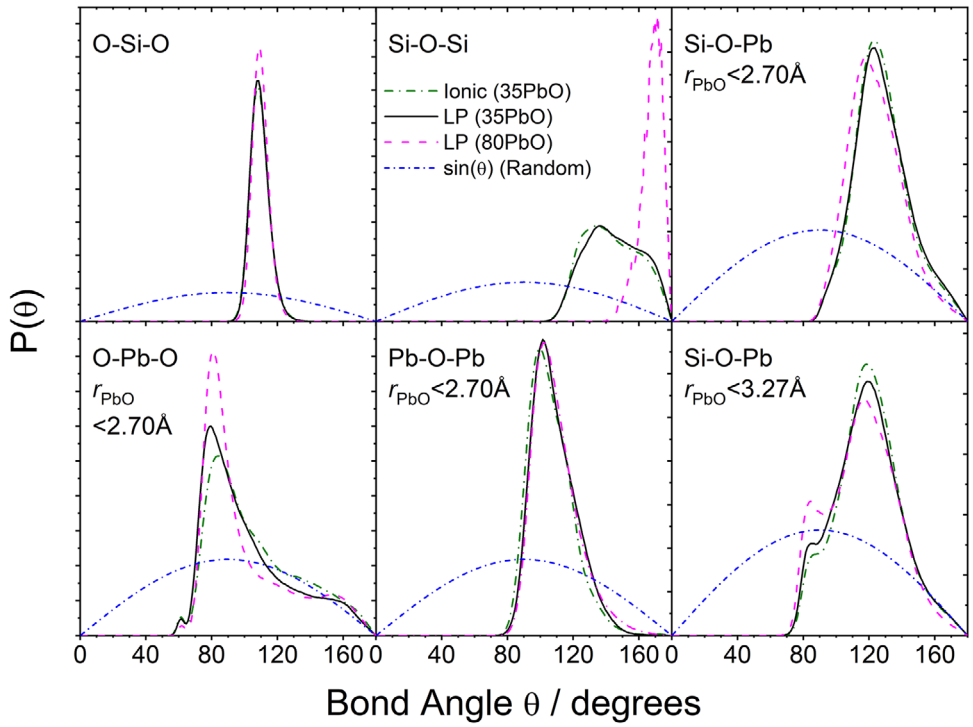

FIGURE 14 Selected bond angle distributions for EPSR models of $35PbO.65SiO_2$ glass and the equivalent distributions for the depolymerized ("Q^0") LP model of $80PbO.20SiO_2$ glass.[2] Only short (≤ 2.7 Å) Pb-O bonds have been included in most instances, and Si-O bonds ≤ 2.0 Å. The Si-O-Si distribution in the LP model of $80PbO.20SiO_2$ glass is not necessarily accurate due to the low weight of the Si-Si partial in the diffraction measurements, and the crude distance-based constraint placed on Si-Si pairs, see Ref[2] for discussion and alternative models. In color online

similar Pb-Pb distances are observed between both edge and corner-sharing [PbO_m] polyhedra.

Mizuno et al.[80] placed the threshold for a percolating plumbite network at between 35 and 50 mol% PbO, based on the dissolution behavior of the glasses. It is interesting to note that in the 35 mol% PbO silicate glass model, based on the Pb-Pb CND, there are very few (~11%) Pb atoms with only one (~2%) or two (~8%) Pb neighbors; the average $n_{PbPb} = 4.65$ ($r_2 = 4.75$ Å) is indicative of a close to fully percolating network. The SAXS intensity, discussed at length by Golubkov et al.,[81] rises sharply below 35 mol% PbO, implying inhomogeneous distributions of Pb atoms. Thus, the dramatic drop in diffusion coefficient, interpreted as a percolation threshold, appears as an observable feature in the SAXS.

Figure 3 shows a peak in SAXS intensity from the $35PbO.65SiO_2$ glass at approximately 0.7 $Å^{-1}$, and this is reproduced to some extent by the models, Figure 16, but shows oscillations due to the limited 39.95 Å box size. Nonetheless, lead-rich regions are visible in the model atom distributions such as that at the top left of Figure 10. A natural mechanism for clustering of Pb, or indeed any modifier, exists which is the requirement of NBOs to be shared by multiple modifier cations. In a simplified model in which Pb(II) is fourfold coordinated, then each NBO should bond to two Pb to provide charge balance, [$OSiPb_2$]. Such a mechanism is at the heart of the modified random network model proposed by Greaves,[82] and it is interesting to speculate that, if the modifier-oxygen coordination number increases, so the NBO-modifier coordination must also increase, along with the size of the modifier-rich clusters/channels. In this way, the morphology of the SAXS should be related to the local structure of the glass, in particular, the cation-oxygen coordination number. Our result shows that SAXS arises in $35PbO.65SiO_2$ glass, despite Pb having low coordination number to oxygen, and hence, behaving more as a network- forming cation. We therefore refute the conclusion of Golubkov et al.[81] who state that the occurrence of SAXS in low lead silicate glasses is "...undoubtedly connected with the structural role of lead which acts here as a modifier of the silicon–oxygen network...," although it is possible that the *peak* in SAXS intensity at 25 mol% PbO may be associated with higher Pb-O coordination and a more modifying role of lead. Nonetheless, the structure of low lead silicate glasses remain unclear due to their high melting temperatures (i.e., difficult to produce) and predicted phase separability (liquid-liquid immiscibility).[49]

An additional low Q feature (prepeak) is observed in the neutron scattering curves of high lead glasses, and has

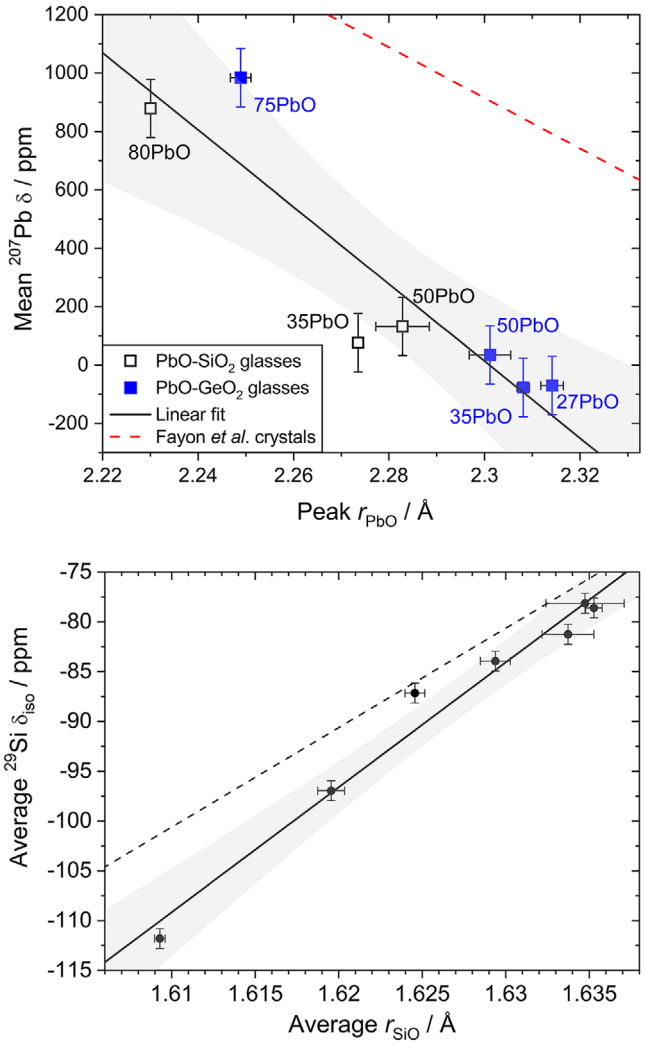

FIGURE 15 Upper: First moments of the ^{207}Pb NMR lineshapes for three lead silicate and four lead germanate[71] glasses, as a function of peak Pb-O bond length measured by neutron diffraction. Molar compositions are indicated on the plot. The solid line is a least-squares fit to the data: $\delta(^{207}\text{Pb}) = -13200\ r_{PbO}(\text{peak}) + 30400$, in ppm and Å (95% confidence bounds shaded), and the dashed line is given by Fayon et al.,[52] $\delta(^{207}\text{Pb}) = -8668.95\ r_{PbO} + 20854$. The main reason for the offset between the two trend lines is attributed to the use of peak (modal) bond lengths herein, which are more easily determined from total scattering data than mean bond lengths, and hence, a more reliable indicator of the local environment. The Fayon et al.,[52] correlation is based on mean bond lengths from crystal structures, not from total scattering. Lower: First moments of the ^{29}Si MAS NMR lineshapes for vitreous silica[88] and lead silicate glasses,[22] as a function of the average Si-O bond length measured by neutron diffraction. The solid line is a least-squares fit to the data: $\delta(^{29}\text{Si}) = 1250\ r_{SiO} - 2130$, in ppm and Å (95% confidence bounds shaded), and the dashed line the composite trend given by MacKenzie and Smith,[79] $\delta_{iso}(^{29}\text{Si}) = 999\ r_{SiO} - 1709$

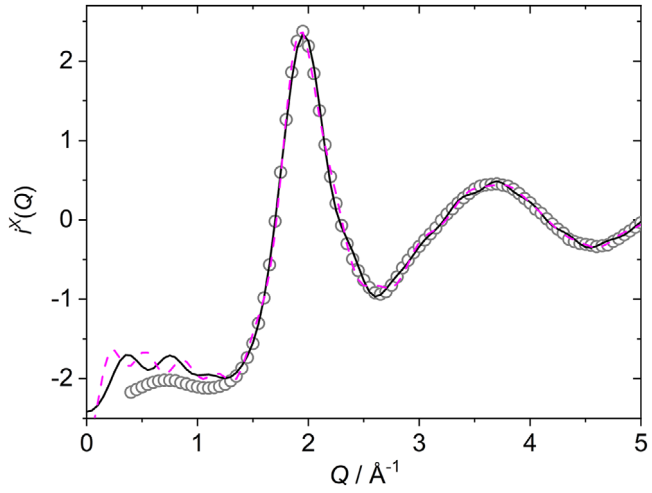

FIGURE 16 Distinct X-ray scattering, at low Q, for 35PbO.65SiO$_2$ glass, showing experimental data (open circles), Ionic (solid black line), and LP (dashed magenta line) models. The ~0.7 Å^{-1} SAXS peak is reproduced to some extent by the 40 × 40 × 40 Å^3, periodically bounded, models

previously been assigned to dispersed silicate anions.[2,3] Figure 4 shows that the increase of the associated periodicity with increasing PbO content is consistent with the silicate anions becoming more dilute. The measured periodicities are greater than the average Si-Si distance calculated as $r_{SiSi} = \rho_{Si}{}^{-1/3}$, with $\rho_{Si} = c_{Si}\rho_0$, which is indicative of residual polymerization, and the retention of some Q^1 species right up to 80 mol% PbO. The increasing correlation length associated with the prepeaks is consistent with that of the FSDPs and the overall increase of intermediate-range order at high PbO contents.

5 | CONCLUSIONS

Over the compositional range 35 to 80 mol% PbO, the local environment of Pb(II) in binary PbO-SiO$_2$ glasses changes only subtly. Pb(II) has a low coordination number to oxygen (~3 to 4), plus a stereochemically active electron LP, and hence, behaves as an oxide glass network forming (or intermediate) cation. This conclusion contradicts conventional wisdom, as well as some of the literature[27,35] in which compositions are proposed at which the role of lead transforms from that of a network modifier to that of a network former. Although such a transformation at compositions with less than 35 mol% PbO is not ruled out, we argue that it is unlikely, especially given the higher molar volumes of lead versus strontium silicate glasses, but requires careful further study.

Subtle changes in the local structure about Pb^{2+} that *do* occur upon increasing from 35 to 80 mol% PbO include:

1. a shortening (of 0.04 Å) and strengthening of the average (short) Pb-O bond, with a concomitant shift of the ^{207}Pb NMR lineshape by +800-900 ppm.
2. an increase of approximately 0.22 in the number of short ($\leq$ 2.70 Å) Pb-O bonds, from 3.3 to 3.6.
3. an increase in site axial symmetry, as evinced by ^{207}Pb NMR CSA lineshapes.

All of these points are consistent with a gradual transition toward axially symmetric square pyramidal [PbO_4] sites, such as those within the crystalline PbO polymorphs.

Even as the local structure about Pb(II) tends toward that in crystalline PbO, so the position of the FSDP increases with increasing PbO content, and the associated periodicity decreases toward that of the β-PbO polymorph. This occurs along with an attendant narrowing of the FSDP, and so an increase in correlation length (up to 19.7(6) Å) and intermediate-range ordering in the glass, which is also evident in the silicate anion ordering. All of these facts have implications for the glass-forming limit in the PbO-SiO_2 system, with crystallization becoming ever easier as the size of the plumbite network regions increase, and their structure becomes more and more similar to β-PbO.

Stereochemically active Pb(II) electron LPs occupy the natural voids within the silicate network at low PbO contents, while at high PbO contents they begin to aggregate within voids that form part of the plumbite network, in analogy to the open channels in $Pb_{11}Si_3O_{17}$ and the layered structures of α- and β-PbO.

Thus, the structural behavior of Pb(II) in lead silicate glasses differs markedly from typical *M*(II) modifiers in alkaline earth silicate glasses, evidence for which can be seen in the glass molar volumes (and atom number densities), by comparison with the ionic radii of the divalent cations, Figure 1.

As an additional point, we note that pulsed neutron total scattering is capable of measuring average bond lengths sufficiently accurately that correlations between Si-O or Pb-O bond lengths, with ^{29}Si or ^{207}Pb NMR chemical shifts respectively, could be measured. This is the first time that such correlations have been demonstrated for a series of glasses.

Our conclusions hold for the rapidly quenched glasses of the present study, and any effects of annealing, or otherwise varying the thermal history, remain an open area for further research.

ACKNOWLEDGMENTS

This work is based on research presented in the doctoral thesis of Oliver L. G. Alderman.[68] This work was funded by the STFC Centre for Materials Physics and Chemistry under Grant CMPC09105 and the EPSRC. We thank the US National Science Foundation for supporting this work under Grant number NSF-DMR 1746230. Uwe Hoppe, Martin v. Zimmerman and Anke Watenphule are gratefully acknowledged for their assistance at beamline BW5, DORIS III, HASYLAB at DESY.

ORCID

Oliver L. G. Alderman https://orcid.org/0000-0002-2342-811X
Alex C. Hannon https://orcid.org/0000-0001-5914-1295

REFERENCES

1. Dumbaugh WH, Lapp JC. Heavy-metal oxide glasses. J Am Ceram Soc. 1992;75(9):2315-26.
2. Alderman OLG, Hannon AC, Holland D, Feller S, Lehr G, Vitale AJ, et al. Lone-pair distribution and plumbite network formation in high lead silicate glass, 80PbO.20SiO_2. Phys Chem Chem Phys. 2013;15(22):8506-19.
3. Kohara S, Ohno H, Takata M, Usuki T, Morita H, Suzuya K, et al. Lead silicate glasses: Binary network-former glasses with large amounts of free volume. Phys Rev B. 2010;82:134209.
4. Takaishi T, Takahashi M, Jin J, Uchino T, Yoko T, Takahashi M. Structural study on PbO-SiO_2 glasses by X-ray and neutron diffraction and Si-29 MAS NMR measurements. J Am Ceram Soc. 2005;88(6):1591-6.
5. Hoppe U, Kranold R, Ghosh A, Landron C, Neuefeind J, Jovari P. Environments of lead cations in oxide glasses probed by X-ray diffraction. J Non-Cryst Solids. 2003;328(1-3):146-56.
6. Suzuya K, Kohara S, Ohno H. A reverse Monte Carlo study of lead metasilicate glass. Japanese J Appl Phys Part 1-Regul Papers Short Notes Rev Papers. 1999;38:144-7.
7. Suzuya K, Price DL, Saboungi ML, Ohno H. Intermediate-range order in lead metasilicate glass. Nucl Instrum Meth B. 1997;133(1-4):57-61.
8. Yamada K, Matsumoto A, Niimura N, Fukunaga T, Hayashi N, Watanabe N. Short-range structural-analysis of lead silicate-glasses by pulsed neutron total scattering. J Phys Soc Jpn. 1986;55(3):831-7.
9. Imaoka M, Hasegawa H, Yasui I. X-ray-diffraction analysis on the structure of the glasses in the system PbO-SiO_2. J Non-Cryst Solids. 1986;85(3):393-412.
10. Morikawa H, Takagi Y, Ohno H. A random network structure model for 2PbO.SiO_2 glass: Reply. J Non-Cryst Solids. 1984;68(1):159-62.
11. Hasegawa H, Imaoka M. Structural-analysis of 2PbO.SiO_2 glass: Comment. J Non-Cryst Solids. 1984;68(1):157-8.
12. Ohno H, Igarashi K, Takagi Y, Toratani H, Furukawa K, Mochinaga J, et al. X-ray-diffraction analysis of glassy and molten states of the PbO-SiO_2 system. J Jpn I Met. 1983;47(2):132-41.
13. Morikawa H, Takagi Y, Ohno H. Structural-analysis of 2PbO.SiO2 glass. J Non-Cryst Solids. 1982;53(1-2):173-82.
14. Imaoka M, Hasegawa A. X-ray diffraction study of 2PbO.SiO_2. J. Ceramic Assoc. Japan. 1980;88(3):141-50.
15. Fayon F, Landron C, Sakurai K, Bessada C, Massiot D. Pb2+ environment in lead silicate glasses probed by Pb-L-III edge XAFS and Pb-207 NMR. J Non-Cryst Solids. 1999;243(1):39-44.

16. Mastelaro VR, Zanotto ED, Lequeux NC, Cortes R. Relationship between short-range order and ease of nucleation in $Na_2Ca_2Si_3O_9$, $CaSiO_3$ and $PbSiO_3$ glasses. J Non-Cryst Solids. 2000;262(1-3):191-9.
17. Rybicki J, Rybicka A, Witkowska A, Bergmanski G, Di Cicco A, Minicucci M, et al. The structure of lead-silicate glasses: Molecular dynamics and EXAFS studies. J Phys: Condens Matter. 2001;13(43):9781-97.
18. Hosono H, Kawazoe H, Kanazawa T. Coordination of Pb^{2+} in oxide glasses determined by ESR and properties of binary lead glasses. J Ceram Assoc Japan. 1982;90(9):544-51.
19. Lippmaa E, Samoson A, Magi M, Teeaar R, Schraml J, Gotz J. High-resolution Si-29 NMR-study of the structure and devitrification of lead-silicate glasses. J Non-Cryst. Solids. 1982;50(2):215-8.
20. Dupree R, Ford N, Holland D. An examination of the Si-29 environment in the PbO-SiO_2 system by magic angle spinning nuclear-magnetic-resonance. 1. Glasses. Phys Chem Glasses. 1987;28(2):78-84.
21. Fayon F, Bessada C, Massiot D, Farnan I, Coutures JP. Si-29 and Pb-207 NMR study of local order in lead silicate glasses. J Non-Cryst Solids. 1998;232:403-8.
22. Feller S, Lodden G, Riley A, Edwards T, Croskrey J, Schue A, et al. A multispectroscopic structural study of lead silicate glasses over an extended range of compositions. J Non-Cryst Solids. 2010;356(6-8):304-13.
23. Lee SK, Kim EJ. Probing metal-bridging oxygen and configurational disorder in amorphous lead silicates: Insights from ^{17}O solid-state nuclear magnetic resonance. J. Phys Chem C. 2015;119(1):748-56.
24. Leventhal L, Bray AJ. Nuclear magnetic resonance investigations of compounds and glasses in the systems PbO-B_2O_3 and PbO-SiO_2. Phys Chem Glasses. 1965;6(4):113-25.
25. Yoko T, Tadanaga K, Miyaji F, Sakka S. A Pb-207 Mas-NMR Study of Pb-containing glasses. J Non-Cryst Solids. 1992;150(1-3):192-6.
26. Smets BMJ, Lommen TPA. The structure of glasses and crystalline compounds in the system PbO-SiO_2, studied by X-ray photo-electron spectroscopy. J. Non-Cryst. Solids. 1982;48(2-3):423-30.
27. Wang PW, Zhang LP. Structural role of lead in lead silicate glasses derived from XPS spectra. J. Non-Cryst. Solids. 1996;194(1-2):129-34.
28. Gee IA, Holland D, McConville CF. Atomic environments in binary lead silicate and ternary alkali lead silicate glasses. Phys. Chem. Glasses. 2001;42(6):339-48.
29. Dalby KN, Nesbitt HW, Zakaznova-Herzog VP, King PL. Resolution of bridging oxygen signals from O 1s spectra of silicate glasses using XPS: Implications for O and Si speciation. Geochim. Cosmochim. Ac. 2007;71(17):4297-313.
30. Nesbitt HW, Bancroft GM, Henderson GS, Sawyer R, Secco RA. Direct and indirect evidence for free oxygen (O^{2-}) in MO-silicate glasses and melts (M= Mg, Ca, Pb). Am Mineral. 2015;100(11-12):2566-78.
31. Furukawa T, Brawer SA, White WB. Structure of lead silicate-glasses determined by vibrational spectroscopy. J Mater Sci. 1978;13(2):268-82.
32. Worrell CA, Henshall T. Vibrational spectroscopic studies of some lead silicate-glasses. J. Non-Cryst. Solids. 1978;29(3):283-99.
33. Piriou B, Arashi H. Raman and infrared investigations of lead silicate-glasses. High Temp Sci. 1980;13(1-4):299-313.
34. Liu LP. Infrared-spectroscopy on lead silicate glass. Z Phys B Con Mat. 1993;90(4):393-9.
35. Meneses DD, Malki M, Echegut P. Structure and lattice dynamics of binary lead silicate glasses investigated by infrared spectroscopy. J. Non-Cryst. Solids. 2006;352(8):769-76.
36. Damodaran KV, Rao BG, Rao KJ. A Molecular-dynamics study of a PbO.SiO_2 glass and melt. Phys. Chem. Glasses. 1990;31(6):212-6.
37. Cormier G, Peres T, Capobianco JA. Molecular dynamics simulation of the structure of undoped and Yb^{3+}-doped lead silicate glass. J. Non-Cryst. Solids. 1996;195(1-2):125-37.
38. Rybicki J, Alda W, Rybicka A, Feliziani S. Structure of lead-silicate glasses via constant-pressure MD simulations. Comput Phys Commun. 1996;97(1-2):191-4.
39. Peres T, Litton DA, Capobianco JA, Garofalini SH. Three-body potential modeling of undoped and Er^{3+}-doped lead silicate glass. J. Non-Cryst. Solids. 1997;221(1):34-46.
40. Peres T, Litton DA, Capobianco JA, Garofalini SH. A multibody potential to study the structure of undoped and Er^{3+}-doped lead silicate glasses. Philos Mag B. 1998;77(2):389-96.
41. Rybicka A, Rybicki J, Witkowska A, Feliziani S, Mancini G. The structure of the first co-ordination shell of Pb atoms in lead-silicate glasses: A molecular dynamics study. Computatl Methods Sci Technol. 1999;5:67-74.
42. Bergmanski G, Bialoskorski M, Rychcik-Leyk M, Witkowska A, Rybicki J, Mancini G, et al. The structure of rarefied and densified $PbSiO_3$ glass: A molecular dynamics study. Task Quarterly. 2004;8(3):393-412.
43. Kato K. Die Kristallstruktur des Bleisilicats $Pb_{11}Si_3O_{17}$. Acta Crystallogr. 1982;B38:57-62.
44. Hill RJ. Refinement of the structure of orthorhombic PbO (Massicot) by Rietveld analysis of neutron powder diffraction data. Acta Crystallogr. C. 1985;41:1281-4.
45. Dickinson RG, Friauf JB. The crystal structure of tetragonal lead monoxide. J Am Chem Soc. 1924;46:2457-63.
46. Stein W-D, Liebertz J, Becker P, Bohatý L, Braden M. Structural investigations of the tetraborates MB_4O_7 (M= Pb, Sr, Ba). Eur Physicl J B. 2012;85(7):236.
47. Takaishi T, Jin JS, Uchino T, Yoko T. Structural study of PbO-B_2O_3 glasses by X-ray diffraction and B-11 MAS NMR techniques. J Am Ceram Soc. 2000;83(10):2543-8.
48. Shaw JL, Werner-Zwanziger U, Zwanziger JW. Correlation of lead borate glass structure with photoelastic response. Phys. Chem. Glasses: Eur. J. Glass Sci. Technol. B. 2006;47(4):513-7.
49. Shevchenko M, Jak E. Experimental phase equilibria studies of the PbO–SiO_2 system. J Am Ceram Soc. 2018;101(1):458-71.
50. Havel AJ, Feller SA, Affatigato M, Karns M, Karns M. Design and operation of a new roller quencher for rapidly cooling melts into glasses. Glass Technol. Eur. J. Glass Sci. Technol. A. 2009;50(4):227-9.
51. Holland D, Feller SA, Kemp TF, Smith ME, Howes AP, Winslow D, et al. Boron-10 NMR: what extra information can it give about borate glasses? Phys Chem Glasses Eur. J Glass Sci Technol B. 2007;48(1):1-8.
52. Fayon F, Farnan I, Bessada C, Coutures J, Massiot D, Coutures JP. Empirical correlations between Pb-207 NMR chemical shifts and structure in solids. J Am Chem Soc. 1997;119(29):6837-43.

53. Hannon AC. Results on disordered materials from the GEneral Materials diffractometer, GEM, at ISIS. Nucl Instrum Meth A. 2005;551(1):88-107.
54. Poulsen HF, Neuefeind J, Neumann HB, Schneider JR, Zeidler MD. Amorphous silica studied by high-energy X-ray-diffraction. J Non-Cryst Solids. 1995;188(1-2):63-74.
55. Bouchard R, Hupfeld D, Lippmann T, Neuefeind J, Neumann HB, Poulsen HF, et al. A triple-crystal diffractometer for high-energy synchrotron radiation at the HASYLAB high-field wiggler beamline BW5. J Synchrotron Radiat. 1998;5:90-101.
56. Bearden JA, Burr AF. Reevaluation of X-ray atomic energy levels. Rev Mod Phys. 1967;39(1):125-42.
57. Hannon AC, Howells WS, Soper AK. Atlas: a suite of programs for the analysis of time-of-flight neutron-diffraction data from liquid and amorphous samples. Inst Phys Conf Ser. 1990;(107):193-211.
58. Finbak C. The structure of liquids .1. Acta Chem Scand. 1949;3(10):1279-92.
59. Waasmaier D, Kirfel A. New analytical scattering-factor functions for free atoms and ions. Acta Crystallogr. A. 1995;51:416-31.
60. Lorch E. Neutron diffraction by germania, silica and radiation-damaged silica glasses. J. Phys. C. 1969;2:229.
61. Sears VF. Neutron scattering lengths and cross sections. Neutron News. 1992;3(3):26-37.
62. Faber T, Ziman J. A theory of the electrical properties of liquid metals. Philos Mag. 1965;11(109):153-73.
63. Keen DA. A comparison of various commonly used correlation functions for describing total scattering. J Appl Crystallogr. 2001;34:172-7.
64. Pirovano C, Islam MS, Vannier RN, Nowogrocki G, Mairesse G. Modelling the crystal structures of Aurivillius phases. Solid State Ion. 2001;140(1-2):115-23.
65. Lebellac D, Kiat JM, Garnier P. Electronic lone-pair localization and electrostatic energy calculations: Application to α-PbO, SnO, $Pb_{1-X}(TiO)_XO$, Pb_3O_4,$Pb_3(V,P)_2O_8$, and a BiSrCaCuO-type superconductor. J Solid State Chem. 1995;114(2):459-68.
66. Massiot D, Fayon F, Capron M, King I, Le Calve S, Alonso B, et al. Modelling one- and two-dimensional solid-state NMR spectra. Magn Reson Chem. 2002;40(1):70-6.
67. Soper AK. Partial structure factors from disordered materials diffraction data: An approach using empirical potential structure refinement. Phys. Rev. B. 2005;72(10):104204.
68. Alderman OLG. The Structure of vitreous binary oxides: Silicate, germanate and plumbite networks. Department of Physics, University of Warwick, Thesis for Ph. D., pp. 254. 2013.
69. Ushida H, Iwadate Y, Hattori T, Nishiyama S, Fukushima K, Ikeda Y, et al. Network structure of B_2O_3-PbO and B_2O_3-PbO-$PbBr_2$ glasses analyzed by pulsed neutron diffraction and Raman spectroscopy. J Alloys Compd. 2004;377(1-2):167-73.
70. Martin V, Wood B, Werner-Zwanziger U, Zwanziger JW. Structural aspects of the photoelastic response in lead borate glasses. J. Non-Cryst. Solids. 2011;357(10):2120-5.
71. Alderman OLG, Hannon AC, Holland D, Dupree R, Feller S. Structural origin of the weak germanate anomaly in lead germanate glass properties. J Am Ceram Soc. 2021. https://doi.org/10.1111/jace.18166
72. Antao SM, Hassan I, Wang J, Lee PL, Toby BH. State-of-the-art high-resolution powder X-ray diffraction (HRPXRD) illustrated with Rietveld structure refinement of quartz, sodalite, tremolite, and meionite. Can Mineral. 2008;46:1501-9.
73. Glasser LSD, Howie RA, Smart RM. The structure of lead orthosilicate, $2PbO.SiO_2$. Acta Crystallogr B. 1981;37:303-6.
74. Petter W, Harnik AB, Keppler U. Crystal structure of lead barysilite, Pb3Si2O7. Z Kristallogr Krist. 1971;133:445-58.
75. Boucher ML, Peacor DR. The crystal structure of alamosite, PbSiO3. Z Kristallogr Krist. 1968;126:98-111.
76. Dove MT, Keen DA, Hannon AC, Swainson IP. Direct measurement of the Si-O bond length and orientational disorder in the high-temperature phase of cristobalite. Phys Chem Miner. 1997;24(4):311-7.
77. Gibbs GV, Hill FC, Boisen MB. The SiO bond and electron density distributions. Phys Chem Miner. 1997;24(3):167-78.
78. Boisen MB, Gibbs GV, Downs RT, Darco P. The dependence of the SiO bond length on structural parameters in coesite, the silica polymorphs, and the clathrasils. Am Mineral. 1990;75(7-8):748-54.
79. Mackenzie KJD, Smith ME. *Multinuclear solid state NMR of inorganic materials* (6). Pergamon: Elsevier; 2002.
80. Mizuno M, Takahashi M, Takaishi T, Yoko T. Leaching of lead and connectivity of plumbate networks in lead silicate glasses. J Am Ceram Soc. 2005;88(10):2908-12.
81. Golubkov VV, Bogdanov VN, Pakhnin AY, Solovyev VA, Zhivaeva EV, Kabanov VO, et al. Microinhomogeneities of glasses of the system PbO-SiO_2. J Chem Phys. 1999;110(10):4897-906.
82. Greaves GN. Exafs and the structure of glass. J. Non-Cryst. Solids. 1985;71(1-3):203-17.
83. SciGlass Professional 7.3. ITC Inc., 2008.
84. Dronskowski R. *Computational chemistry of solid state materials* (300). New York, NY: Wiley Online Library; 2005.
85. Barney ER, Hannon AC, Holland D, Winslow D, Rijal B, Affatigato M, et al. Structural studies of lead aluminate glasses. J. Non-Cryst. Solids. 2007;353(18-21):1741-7.
86. Hannon AC, Parker JM, Vessal B. Neutron diffraction analysis of the atomic short range order in lead gallate glasses. J. Non-Cryst. Solids. 1998;232:51-8.
87. Hannon AC, Parker JM, Vessal B. The effect of composition in lead gallate glasses: A structural study. J. Non-Cryst. Solids. 1996;196:187-92.
88. Malfait WJ, Halter WE, Verel R. ^{29}Si NMR spectroscopy of silica glass: T_1 relaxation and constraints on the Si–O–Si bond angle distribution. Chem Geol. 2008;256(3–4):269-77.

SUPPORTING INFORMATION

Additional supporting information may be found in the online version of the article at the publisher's website.

How to cite this article: Alderman OLG, Hannon AC, Holland D, Dupree R, Lehr G, Vitale A, Feller S. Lead silicate glass structure: New insights from diffraction and modeling of probable lone pair locations. J Am Ceram Soc. 2022;105:938–957. https://doi.org/10.1111/jace.18125